Evaluating sediments as an ecosystem service in western Lake Erie via quantification of nutrient cycling pathways and selected gene abundances

Ashlynn R. Boedecker[a,1,*], Desi N. Niewinski[a,2], Silvia E. Newell[a], Justin D. Chaffin[b], and Mark J. McCarthy[a]

[a]Department of Earth and Environmental Sciences, Wright State University, 3640 Colonel Glenn Hwy, Dayton, OH 45435, USA

[b]F. T. Stone Laboratory and Ohio Sea Grant, The Ohio State University, 878 Bayview Ave, P.O. Box 119, Put-In-Bay, OH 43456, USA

[1]Present address: Department of Biology, Baylor University, One Bear Place, Waco, TX 76798, USA

[2]Present address: Mary Griggs Burke Center for Freshwater Innovation, Northland College, 1411 Ellis Ave S, Ashland, WI 54806, USA

*Corresponding author: ashlynn_boedecker2@baylor.edu (A.R. Boedecker)

Abstract

Lake Erie experiences annual summer cyanobacterial harmful algal blooms (HABs), comprised mostly of non-nitrogen-fixing *Microcystis* due to excess nitrogen (N) and phosphorus (P) inputs (eutrophication). Lake Erie's watershed is mostly agricultural; and fertilizers, manure, and drainage practices contribute to high nutrient loads. This study aimed to clarify the role of western Lake Erie sediments in either exacerbating or mitigating conditions that fuel HABs via recycling and/or removal, respectively, of excess N and reactive P. Sediment-water interface N and ortho-P dynamics and functional gene analyses of key N transformations were evaluated during a dry, low HAB year (2016) and a wet, high HAB year (2017). On average, western basin sediments were a net N sink and thus perform a valuable ecosystem service via N removal. However, sediments were a source of ortho-P and chemically reduced N. Western basin sediments can theoretically remove 29% of average annual watershed total N loading. However, denitrification rates were lower during the high (2017) versus low bloom years (2016), suggesting that high external N loading and large HABs inhibit the capacity of sediments to perform that ecosystem service. Despite being a net N sink on average, western basin sediments released ammonium and urea, chemically reduced N forms that are energetically conducive to non-N-fixing, toxin-producing cyanobacterial HABs, especially during the critical period of low external loading and high biomass. These results support other recent work highlighting the urgent need to include N cycling and internal load dynamics in ecosystem models and mitigation efforts for eutrophic systems.

Keywords: Nutrients, Denitrification, Nitrogen fixation, Harmful algal blooms

Introduction

Since the mid-1990s, Lake Erie has experienced toxic cyanobacterial harmful algal blooms (HABs) due to high nutrient (nitrogen (N) and phosphorus (P)) inputs from its tributaries (Murphy et al., 2003). These blooms negatively affect aquatic life, pets, livestock, and humans, as evidenced by the shutdown of the city of Toledo, Ohio, water treatment plant in August 2014 due to high cyanotoxin levels (Carmichael and Boyer, 2016). Contemporary HABs in the western basin of Lake Erie are mostly composed of cyanobacterial taxa (*Microcystis*) that cannot fix atmospheric N. This community structure differs from HABs observed in Lake Erie in the 1960s and 1970s, which were capable of N fixation (Steffen et al., 2014; Chaffin et al., 2018a). The watershed of the western basin is mostly agricultural, and associated fertilizer, manure, and drainage practices within the Maumee River watershed contribute to high nutrient loads entering the western basin (Moog and Whiting, 2002; Stumpf et al., 2012; Verhamme et al., 2016).

The yearly average total N load entering the western basin from the Maumee River is about 38,500 metric tons (33-year average; Richards et al., 2010). The Ohio EPA (2018) reported the yearly average TN load between 2013 and 2017 to be 41,146 metric tons, but 2017 was an unusually high load year and contributed to the major increase. However, even though total N loads are mostly remaining consistent, the proportion of the Maumee river total N load comprised of total Kjeldahl N (TKN; non-nitrate/nitrite N, including chemically reduced forms, such as ammonium (NH_4^+), urea, and other labile organic N) is also increasing relative to

oxidized inorganic N (NO_x; Newell et al., 2019). Phytoplankton community structure can shift from favoring diatoms in nitrate (NO_3^-) dominated waters to cyanobacteria in NH_4^+ dominated waters (McCarthy et al., 2009; Glibert et al., 2016), which often corresponds to a shift in trophic status. Different forms of N (e.g., NH_4^+ and urea) can also contribute to the toxicity of HABs (Donald et al., 2011; Davis et al., 2015). In the 1980s – 1990s, the predominant N form in fertilizers switched from NH_4NO_3 to UAN (urea ammonium nitrate; Glibert et al. 2006, 2014; Paerl et al., 2016). Urea is an organic N form that is bioavailable and energetically favorable for cyanobacteria (Glibert et al. 2014; Belisle et al. 2016) and can exacerbate HABs in the receiving waters of agricultural watersheds.

Many studies (e.g., Han et al., 2012; Bridgeman et al., 2013; Baker et al., 2014; Kane et al., 2014; Stow et al., 2015) have linked nutrient loads from the Maumee River to HABs in Lake Erie; however, few studies have addressed the transformations, internal loads, and ultimate fate of N within the lake or sediments. Sediments receiving labile organic matter from the overlying water column can exacerbate oxygen drawdown and contribute to water column hypoxia and internal nutrient loading. As organic matter is decomposed, dissolved oxygen (DO) is respired, and ortho-phosphate (ortho-P) and NH_4^+ can be released. Sediments can also store N and P for long periods, making them an important source for legacy nutrient loading (Heisler et al., 2008). Many studies show that Lake Erie sediments are a consistent source of P to the water column (Holdren and Armstrong, 1980; Matisoff et al., 2016; Watson et al., 2016; Paytan et al., 2017). Gross sediment N fluxes have been reported in Sandusky Bay (Salk et al., 2018) and Old Woman Creek (McCarthy et al., 2007), two coastal Lake Erie subsystems, and Small et al. (2014) reported sediment N fluxes from a single sampling event within the western basin. These studies

provide some baseline knowledge, but more work is clearly needed to understand the ecological role of sediment N transformations in Lake Erie.

The overall objective of this study was to determine the extent to which western basin sediments act as a source or sink for reactive N and P. Rates and pathways of N fluxes and transformations and ortho-P fluxes at the sediment-water interface were identified and quantified using intact sediment core incubations. N removal rates via denitrification and/or anammox were measured, as well as fluxes of combined N forms (i.e., NH_4^+, NO_3^-, NO_2^-, urea) and DO across the sediment-water interface. The rate of sediment N fixation occurring simultaneously with denitrification was calculated from isotopic measurements, and abundances of selected N cycling genes (*nirS* and *nifH*, encoding denitrification and N fixation, respectively) were evaluated to support the core incubation results. We hypothesized that: (1) sediments are a net source of chemically reduced N (NH_4^+ and urea) and ortho-P to the system; (2) denitrification is the major N loss pathway, with a small fraction lost via possible anammox; and (3) net denitrification occurs in the spring through mid-summer, then switches to net N fixation in the late summer to early fall.

Methods

Study sites and field sampling

Water samples and intact sediment cores were collected from four locations along the Maumee River discharge gradient in western Lake Erie during the ice-free seasons (April – October) of 2016 and 2017 (Figure 1). The sampling gradient began in Maumee Bay and extended towards the center of the basin. Water depths increased with distance from the river mouth (MB18 = 2.5 m, WE2 = 5 m, WE4 = 8 m, and WE13 = 8.5 m). MB18 and WE2 were

sampled in July, August, September, and October 2016 and April, July, August, and October 2017. WE4 and WE13 were sampled in May, June, August, and October 2016 and June, July, August, and October 2017.

Surface and bottom water (~1 m above sediment) samples were collected using a 7 L Niskin bottle and filtered immediately, on location, using 0.2 μm syringe filters for ambient nutrient analyses. All nutrient samples were stored on ice for transport and frozen at -20°C until analysis. For each of the sediment core incubations, six intact sediment cores were collected using a custom sediment coring lander designed to maintain sediment core (7.6 cm diameter, ~15 cm depth) and overlying water integrity (Gardner et al., 2009). Along with intact sediment cores, ~60 L of bottom water was collected in three, pre-rinsed, 20 L cubitainers. After collection, cores were sealed at both ends with a vinyl cap and stored in a dark cooler until incubations commenced (within 8 hours of collection).

Sediment core incubation and analysis

To prepare sediment cores for incubation, overlying water was decanted, being careful not to disturb the sediment-water interface, until about 10 cm of overlying water remained above the sediment surface. An air-and-water tight plunger fitted with gastight inflow and outflow tubing (PEEK) was pushed into the core tube until the inflow line was about 1 cm above the sediment-water interface (Lavrentyev et al., 2000; Gardner and McCarthy, 2009). Each sediment core was wrapped in aluminum foil to prevent light effects. Two 8-channel peristaltic pumps were used to supply the overlying core water with a constant flow of unfiltered reservoir water. Because the western basin is well-mixed and does not usually experience bottom-water hypoxia, aquarium bubblers were used to maintain reservoir water at atmospheric equilibrium throughout

the incubation. Sediment cores were incubated at ~20°C, reflecting a general average of in situ bottom water temperatures over the sampling season. Previous work has shown that our incubation approach maintains *in situ* redox dynamics as well as an intact microbial community (Bernot et al., 2003).

Nitrogen removal and recycling rates were measured using a well-established, continuous-flow protocol (e.g., An et al., 2001; Gardner et al., 2006; McCarthy et al., 2007; McCarthy et al., 2015; McCarthy et al., 2016; McTigue et al., 2016; Hoffman et al., 2019). Treatments for each incubation included duplicate cores for: (1) unamended control for net $^{28}N_2$, net DO (sediment oxygen demand), and nutrient (NH_4^+, NO_2^-, NO_3^-, urea, and ortho-P) fluxes; (2) $^{15}NH_4^+$ tracer addition for possible anammox rates; and (3) $^{15}NO_3^-$ tracer addition for potential denitrification, dissimilatory NO_3^- reduction to NH_4^+ (DNRA), and N fixation rates. Reservoir water flowed into the overlying water column of each core at ~1.35 mL/min (water residence time ~5 h; An et al., 2001). Once continuous-flow was initiated, sampling commenced at least 12 hours later to allow the system to establish steady-state. Nutrient and dissolved gas samples were collected once daily for three days from both inflow reservoirs and outflows to determine fluxes and transformation rates.

Dissolved gas samples were analyzed immediately for $^{28,29,30}N_2$, O_2, and Ar using membrane inlet mass spectrometry (MIMS; Kana et al., 1994; An et al., 2001). When core incubations were conducted remotely (August 3-6, 2016, and July 11-13, 2017), dissolved gas samples were collected to overflowing in 15 mL ground-glass stoppered test tubes (Chemglass), preserved with 200 µL of 50% (w/v) $ZnCl_2$, stored submerged in 4 L Nalgene bottles, and analyzed within one week using MIMS (McCarthy et al., 2015). After collection, filtered nutrient

samples were frozen at -20°C until analysis on a Lachat QuikChem 8500 Flow Injection Analysis system using manufacturer protocols.

Data Calculations

Maumee River discharge rates and loading data (including nutrient concentrations) from 2016 and 2017 were obtained from Heidelberg University's National Center for Water Quality Research in May 2019 (NCWQR; www.heidelberg.edu/academics/research-and-centers/national-center-for-water-quality-research).

Dissolved gas and nutrient fluxes were calculated for each core and sampling event (n = 6 per incubation and treatment). A positive $^{28}N_2$ flux (net N_2 production) in unamended cores indicated that the combination of denitrification and anammox exceeded N fixation, and vice versa. The sum of the fluxes of all N_2 species ($^{28,29,30}N_2$), plus any calculated N fixation occurring simultaneously (calculated from $^{15}NO_3^-$-amended cores; An et al., 2001), represented potential denitrification. In $^{15}NH_4^+$-amended cores, a positive $^{29}N_2$ flux indicated possible anammox. We refer to "possible anammox" because the production of $^{29}N_2$ via anammox cannot be distinguished in our system from nitrification of added $^{15}NH_4^+$ to $^{15}NO_x$ combined via denitrification with *in situ* $^{14}NO_x$ to form $^{29}N_2$ (Hoffman et al., 2019). We used the NO_3^--induced NH_4^+ flux approach (NIAF; see McCarthy et al., 2016) as an indirect proxy for DNRA in Lake Erie sediments.

Dissolved gas concentrations (N_2, O_2, and Ar) were calculated using temperature-controlled water bath standards at 20°C and 30°C. These standards were compared with saturation tables of the dissolved gases at those temperatures, and measured signals were corrected for instrument drift (Kana et al., 1994). The instrument drift calculated from air-

saturated standards was used to adjust N_2/Ar and O_2/Ar measurements, and the resulting ratios were multiplied by the saturation concentration of Ar at 20°C (the temperature of the water bath containing the MIMS inlet) to obtain N_2 and O_2 concentrations (Kana et al., 1994). The MIMS used in this study does not exhibit the oxygen effect observed by Eyre et al., (2002) and does not require installation of a furnace to neutralize this effect (Kana and Weiss, 2004). The signal at mass 30 is constantly monitored during sample analyses, and no significant (relative to analytical precision) mass 30 production was observed in unamended cores throughout the study. Also note that the incubation system used here violates several assumptions (see Eyre et al., 2002) of the isotope pairing technique for estimating denitrification (Nielsen 1992) and thus cannot be applied to our results (Hoffman et al., 2019).

Fluxes were calculated (Lavrentyev et al., 2000) by subtracting inflow solute concentrations from outflow concentrations and dividing by the water flow rate (measured daily, L/hr) multiplied by sediment core surface area (0.0045 m^2; Lavrentyev et al., 2000; McCarthy et al., 2016). A negative flux indicated movement of solute into sediments, and a positive flux represented efflux out of sediments into overlying water. Fluxes of $^{28,29,30}N_2$ were then used, along with the abundances of $^{29,30}N_2$ relative to the total N_2 pool, to calculate N fixation and denitrification simultaneously (An et al., 2001).

Functional gene analysis

Quantitative PCR (qPCR) functional gene analysis was conducted from sediment subsamples collected during each sampling event. Subcores were collected in the field using 10 or 20 mL cut-off syringes, pre-treated with DNA Away (Thermo-Fisher) to prevent nucleic acid contamination, and stored at -80°C until analysis. DNA was extracted using the MoBio

PowerSoil Total RNA Isolation kit and the DNA Elution Accessory, according to manufacturer instructions. Functional gene subunits for denitrification (*nirS* – NO_2^- reductase) and N fixation (*nifH* – nitrogenase) were quantified.

Plasmid standards for qPCR were constructed from cleaned and cloned PCR amplicons. PCR temperature protocols, along with primer names and sequences, are described in Electronic Supplementary Material (ESM) Table S2. The *nirS* PCR reaction contained 2 µL DreamTaq Green buffer (Fisher Scientific), 2 µL of 10 µM primer, 50 ng/µL DNA, and nuclease-free water per 20 µL reaction. The *nifH* PCR reaction contained 2 µL DreamTaq Green buffer, 2 µL of 2 mM dNTP, 0.25 µL DreamTaq enzyme, 2.5 µL of 10 µM primer, 100 ng/µL DNA, and nuclease free water to complete a 20 µL reaction. Amplicons were visualized via electrophoresis in a 1% agarose gel, and PCR bands corresponding to the amplicon length were excised and cleaned using the Promega Wizard SV Gel and PCR Clean-up System. Cleaned product was then cloned into *E. coli* using the TOPO vector kit (Invitrogen) according to manufacturer instructions, and the resulting plasmid was isolated and cleaned using the MoBio UltraClean Standard Mini Plasmid Prep kit.

qPCR analysis followed the temperature protocols shown in ESM Table S2. The qPCR reaction included 10 µL Fast SYBR Green, 2 µL of 10 µM primer, 20 ng/µL DNA, and nuclease free water to complete a 20 µL reaction for *nirS,* and 10 µL Fast SYBR Green, 2.5 µL of 10 µM primer, 40 ng/µL DNA, and nuclease free water to complete a 20 µL reaction for *nifH*. Each assay contained triplicates of the no template controls, six standards, and each sample. Amplicon specificity was confirmed by melting curve analysis. Copies of the functional gene per 20 to 40 ng of DNA were quantified from the standard curve threshold cycle (Ct) values when the r^2 was at least 0.985, efficiency was between 0.9 and 1.1, and negative

controls were not detected during the reaction. Gene copy numbers were quantified (Newell et al., 2016) and converted to gene copy numbers per gram (wet weight) of sediment.

Statistical Analyses

Statistics were performed in R (version 3.6.2, R Core Team) using Spearman's Rank Correlation Coefficient (ρ) in the ggpubr package (Kassambara, 2018) to evaluate correlations as data were not normally distributed (ESM Table S1). Comparisons of variables between the different sites in 2016 and 2017 were conducted using a one-way ANOVA with a Tukey's post-hoc analysis (car package; Fox and Weisberg, 2019).

Results

Ambient nutrients

Sonde measurements, including temperature, dissolved oxygen (DO), and chl-*a* fluorescence, are shown in Table 1. There was no difference between surface and bottom temperatures (ANOVA, $p = 0.68$) or DO concentrations ($p = 0.20$), indicating no water column stratification or hypoxia throughout the two sampling seasons. There was also no difference between surface and bottom water chl-*a* concentrations ($p = 0.58$).

Overall, ambient nutrient concentrations (Table 2) were higher in 2017 than in 2016, and highest concentrations generally occurred earlier in the season. In 2016, surface water NH_4^+ concentrations ranged from 0.086 µM at WE2 on July 13 to 5.95 µM at MB18 on August 3. Bottom water NH_4^+ concentrations ranged from 0.226 µM at WE2 on October 17 to 7.87 µM at WE2 on September 19. In 2017, both surface and bottom water NH_4^+ concentrations ranged from below the detection limit (0.04 µM) at MB18 on October 3 to 7.24 µM at the surface and 7.27

µM at the bottom on July 11, also at MB18. NO_2^- was always detectable in both surface and bottom water samples but was usually less than 3 µM (Table 2). Exceptions occurred on May 18, 2016, when surface and bottom water samples at WE4 and WE13 were 7.29 µM, and on July 11, 2017, at MB18, when surface and bottom waters had NO_2^- concentration of 11.2 µM and 10.8 µM, respectively.

Nitrate concentrations were the most variable and not different between depths (ANOVA; $p = 0.948$), but there was a difference between years (ANOVA; $p = 0.007$). In 2016, surface water NO_3^- concentrations ranged from 1.62 µM at WE13 on August 10 to 53.4 µM at MB18 on July 13, and bottom water concentrations ranged from 2.75 µM at WE13 on August 10 to 66.1 µM at MB18 on August 3. In 2017, surface and bottom water NO_3^- concentrations ranged from 0.014 and 0.078 µM, respectively, at MB18 on October 3, to 487 and 481 µM, respectively, at MB18 on July 11. Urea concentrations were higher in 2016 than 2017 (Table 2). In 2016, surface water urea concentrations ranged from 0.279 µM at WE13 on May 18 and MB18 on August 3 to 6.20 µM at MB18 on July 13. Bottom water urea concentrations ranged from 0.414 µM at WE13 on May 18 to 2.15 µM at MB18 on September 19. In 2017, surface water urea concentrations ranged from 0.304 µM at WE13 on August 2 to 4.95 at MB18 on July 11, and bottom water concentrations ranged from 0.289 µM at WE4 on October 20 to 6.18 µM at MB18 on August 9.

Surface and bottom water concentrations of ortho-P were not different between depths or years. In 2016, surface and bottom water concentrations of ortho-P ranged from 0.025 at WE4 on June 28 to 1.13 µM at WE13 on October 3 (Table 2). In 2017, surface water ortho-P concentrations ranged from 0.010 µM at WE4 on June 9 to 1.76 µM at MB18 on July 11, and

bottom water concentrations ranged from 0.028 µM at WE13 on July 14 to 1.94 µM at MB18 on July 11.

Sediment oxygen demand (SOD)

SOD generally decreased with distance from the river mouth; however, in October 2017, WE13 had the highest SOD, and MB18 and WE2 had the lowest. SOD ranged from 312 ± 12.8 µmol $O_2/m^2/hr$ at WE13 in July 2017 to 2160 ± 291 µmol $O_2/m^2/hr$ at MB18 in July 2017 (Figure 3). SOD at MB18 was higher than at WE2, WE4, and WE13 (ANOVA; $p < 0.001$). SOD was positively correlated with net NH_4^+ ($\rho = 0.792$, $p < 0.001$) and ortho-P fluxes ($\rho = 0.728$; $p < 0.001$) but negatively correlated with net NO_3^- fluxes ($\rho = -0.360$; $p = 0.044$).

Sediment-water interface nutrient fluxes

Bioavailable dissolved N fluxes (NH_4^+; NO_2^-, NO_3^-, urea; Figure 2; Table 3) were obtained from unamended cores, where positive values indicate nutrient release from sediments, and negative values represent influx from overlying water into sediments. In 2016, sediments were, on average, a net NH_4^+ source at all sites, whereas 2017 had lower average net NH_4^+ fluxes, and WE13 was a net NH_4^+ sink. The largest efflux occurred in September 2016 at MB18 (154 ± 22.1 µmol $N/m^2/hr$), and the largest NH_4^+ influx was observed in August 2017 at site WE4 (-12.9 ± 6.90 µmol $N/m^2/hr$). Net NH_4^+ fluxes were significantly greater at MB18 than at WE2 and WE13 (ANOVA; $p = 0.003$).

Sediments usually exhibited net NO_3^- uptake in unamended cores, but low rates of efflux also occurred on some occasions. Lower fluxes (e.g., < 50 µmol $N/m^2/hr$) were often characterized by large variability, with duplicate cores sometimes exhibiting opposite NO_3^- flux

directions. Net NO_3^- fluxes ranged from -222 ± 117 µmol N/m^2/hr at MB18 in July 2017 to 22.4 ± 7.42 µmol N/m^2/hr at MB18 in October 2017. Net NO_3^- fluxes were different between MB18 and WE2 (ANOVA; $p = 0.005$). Net NO_3^- fluxes were negatively correlated with net NH_4^+ fluxes ($\rho = -0.464$; $p = 0.008$; Table S3). Net NO_2^- flux direction was variable in unamended cores, but both net NO_2^- uptake and efflux generally occurred at low rates in both years. The largest net NO_2^- uptake occurred in July 2017 at MB18 (-31.5 ± 11.5 µmol N/m^2/hr), and the largest net efflux occurred in October 2016 at MB18 (8.12 ± 2.96 µmol N/m^2/hr).

The direction of net urea fluxes varied at all sites except MB18, which always exhibited net efflux. In both years, however, sediments were, on average, a net source of urea at all sites (Table 3). Net urea effluxes peaked at MB18 in July 2017 (26.5 ± 7.13 µmol N/m^2/hr) and were negatively correlated with net NO_3^- fluxes ($\rho = -0.454$; $p = 0.009$; ESM Table S3) and positively correlated with net NH_4^+ fluxes ($\rho = 0.477$; $p = 0.006$).

In 2016, sediments were a net source of ortho-P (Table 3) at all sites and times except WE13 in June and October. In 2017, sediments were a net source of ortho-P at all sites and times. Net ortho-P fluxes generally decreased from Maumee Bay into the western basin. The largest ortho-P efflux occurred at MB18 in July 2017 (13.0 ± 2.06 µmol P/m^2/hr). Net ortho-P fluxes were significantly higher at MB18 than at all other sites (ANOVA; $p < 0.001$), and positively correlated with net NH_4^+ fluxes ($\rho = 0.624$; $p < 0.001$; Table S3).

N_2 transformations

Net N_2 fluxes are reported as either negative (net N fixation) or positive (net denitrification) values. Both processes occur simultaneously (An et al., 2001), and the net value represents the relative balance between them. Using net $^{28}N_2$ fluxes from unamended cores,

along with calculated N fixation rates from $^{15}NO_3^-$ cores, the best estimate of *in situ* denitrification was determined by adding the calculated N fixation rate, if any, to net $^{28}N_2$ fluxes (Figure 4a). Net N fixation was observed at MB18 in July 2016 (-166 μmol N/m^2/hr), WE2 in April 2017 (-25.5 μmol N/m^2/hr), and WE4 in May 2016 (-30.6 μmol N/m^2/hr) and June 2017 (-13.9 μmol N/m^2/hr). All other sites and dates showed net denitrification. However, mean best estimate denitrification rates for each site over both years were all positive, confirming that western basin sediments acted as an overall net N sink.

Potential denitrification (Figure 4b) was determined as the sum of $^{28,29,30}N_2$ production plus any calculated N fixation in $^{15}NO_3^-$ amended cores. On average, potential denitrification was higher at every site in 2016 than 2017, and 2016 had higher average potential denitrification rates overall (180 ± 22.4 μmol N/m^2/hr) than 2017 (84.5 ± 17.4 μmol N/m^2/hr; ANOVA, $p = 0.003$). Potential denitrification and the best estimate of *in situ* denitrification were not different ($p = 0.124$), indicating that sediment denitrifiers were generally operating at capacity and could not accelerate N_2 production at higher N loads. Potential denitrification was positively correlated with net ortho-P flux ($\rho = 0.386$; $p = 0.029$; ESM Table S3), net NH_4^+ flux ($\rho = 0.488$; $p = 0.005$), and SOD ($\rho = 0.792$; $p < 0.001$) from unamended cores. Production of $^{29}N_2$ from $^{15}NH_4^+$ amendments (possible anammox) ranged from 0.43 to 32.4 μmol N/m^2/hr (data not shown). Across all sites, possible anammox contributed an average of 14% of total N_2 release from sediments, with a maximum of 47% in October 2017 at WE2 (data not shown).

Calculated N fixation (Figure 4c) did not differ between 2016 and 2017. When detected, sediment N fixation rates ranged from 6.30 ± 3.62 μmol N/m^2/hr at WE2 in October 2017 to 239 ± 119 μmol N/m^2/hr at WE4 in June 2016. There were also no differences between sites (ANOVA, $p = 0.33$). Calculated N fixation rates were positively correlated with SOD ($\rho = 0.355$;

p = 0.046; ESM Table S3) but negatively correlated with net NO_3^- flux (ρ = -0.423; p = 0.016) from unamended cores.

Functional gene analysis

Functional gene abundances were calculated in terms of genes per gram of wet sediment. The average water content of the sediment was 43.6%. Denitrifier abundance (Figure 5a), calculated using *nirS* gene abundance as a proxy, was higher in 2016 than 2017 (ANOVA, p < 0.001). Gene copy numbers in 2016 ranged from 7.35 x 10^{10} to 1.5 x 10^{12} copies *nirS*/g sediment. Copies in 2017 ranged from 5.09 x 10^9 to 1.07 x 10^{11} copies *nirS*/g sediment. The greatest abundance of *nirS* copies was observed at MB18 in all cases except July 2017, when WE2 had the most gene copies. Copy numbers generally decreased from spring to late summer for MB18 and WE2, but the opposite trend was observed at WE4 and WE13. Sediment *nirS* copies were positively correlated with potential denitrification rates (ρ = 0.597, p < 0.001; ESM Table S3).

Gene copies of *nifH* (Figure 5b) in sediments were quantified as a proxy for (likely heterotrophic) N fixers. Abundance of the *nifH* gene was higher in 2017 versus 2016 (ANOVA, p = 0.018). Copies of *nifH* ranged from 6.57 x 10^6 to 3.73 x 10^9 copies *nifH*/g sediment in 2016 and 1.24 x 10^7 to 1.04 x 10^{10} copies *nifH*/g sediment in 2017. Like *nirS*, copies of *nifH* were higher at MB18 in all cases except July 2017, when WE13 exhibited the most *nifH* copies. No relationship was observed between *nifH* gene copies and calculated N fixation rates (ρ = 0.249, p = 0.177). However, *nifH* gene copies were negatively correlated to the best estimate of denitrification in unamended cores (ρ = -0.383, p = 0.034).

Discussion

This study showed that sediments in western Lake Erie play a key role in aerobic and anaerobic nutrient cycling, which are important factors driving phytoplankton community structure and biomass (Forsberg, 1989). Even in lakes where bottom waters are not hypoxic, the oxic-anoxic interface can occur very near the sediment surface, especially in highly productive, eutrophic lakes, making anaerobic processes very pertinent (Brune et al., 2000). Maumee River nutrient loads drive water column productivity and HABs (Baker et al., 2014; Kane et al., 2014; Stow et al., 2015), as well as internal nutrient cycling within the sediments and water column. Precipitation amounts (ESM Figure S1a) and Maumee River discharge rates (ESM Figure S1b) were higher in 2017 (larger bloom) than in 2016 (smaller bloom), which led to higher suspended sediment and nutrient loads. Temperature can also affect internal nutrient cycling (Seitzinger, 1988). Average water temperatures were higher in 2016 (21.5°C) than in 2017 (20.6°C), which coincided with higher average *in situ* denitrification rates. Higher nutrient loads perpetuate HABs (Paerl and Otten, 2013), but the overall effect of higher loading on sediment nutrient dynamics is not fully understood. Determining whether sediments are a net source or sink of reactive N and P, both temporally and spatially, and understanding the physical-biogeochemical mechanisms involved, are imperative for building modern ecosystem models that can be used to help resolve eutrophication and HABs.

Sediment oxygen demand (SOD)

SOD can be used as a proxy for microbial remineralization of organic-rich detritus (e.g., Seiki et al., 1994). In western basin sediments, average SOD typically decreased with increased distance from the river mouth. SOD was also higher in 2016 than in 2017 (ANOVA, $p = 0.005$), which could be explained in part by differences in phytoplankton community composition. In

2016, the *Microcystis* bloom was less extensive than in 2017 (Chaffin et al., 2018b), and phytoplankton FluoroProbe data from the NOAA western basin monitoring program showed that diatoms comprised 35% of the total phytoplankton biomass in 2016, versus only 14% in 2017 (David Fanslow, NOAA-GLERL, personal communication). Diatoms rapidly sink to the benthos, where they provide organic matter for remineralization (Smetacek, 1985). In contrast, cyanobacteria biomass, especially colony-forming species, is often remineralized in the water column (Gardner and Lee, 1975), which could lead to lower denitrification and P burial rates at the sediment – water interface. Denitrification and P burial are important ecosystem services provided by lacustrine sediments, and disruption of these services (e.g., via benthic-pelagic decoupling; Carrick et al., 2005) could further exacerbate eutrophication.

Differences in system residence time relative to transport of organic matter from the western to central basin may also play a role in observed SOD patterns. Precipitation and discharge volumes were higher in 2017 than 2016, likely resulting in shorter residence times in 2017 (Romo et al., 2013). Therefore, labile organic matter (biomass) may have been transported farther into the western and central basins in 2017. This pattern was observed during the 2011 *Microcystis* bloom, which was transported into the central basin (Michalak et al., 2013). SOD typically decreases with increasing water depth because less organic matter reaches the sediment-water interface due to water column remineralization (Clough et al., 2005), especially during HABs (Gardner and Lee, 1975), and this relationship was also observed within the western basin. In 2016, we speculate that the relatively lower cyanobacteria biomass, in conjunction with the higher proportion of diatoms and longer residence time, promoted delivery of phytoplankton biomass to western basin sediments, resulting in higher SOD. In contrast,

disruption of benthic-pelagic coupling in 2017, via phytoplankton community structural changes in conjunction with a shorter residence time, resulted in lower observed SOD.

Sediment nutrient fluxes

Unamended cores were used to characterize overall nutrient fluxes (Table 3) from western Lake Erie sediments. While there was not a distinct spatial pattern between dissolved nutrient fluxes, MB18 always had the largest flux for every measured nutrient, whether positive or negative. Even when sediments were a net sink for dissolved water column N, NH_4^+ and urea were released from the sediments into overlying water, most likely due to organic matter remineralization (Berman et al., 1999). These internal sources of chemically reduced could help maintain phytoplankton and HAB growth. NH_4^+ is the most energetically favorable N form for primary producers, including cyanobacteria (Glibert et al., 2016), and cellular NH_4^+ deficiency stimulates assimilation of other N forms (Herrero et al., 2001). Cyanobacteria can also outcompete other phytoplankton and microbes for NH_4^+ (Blomqvist et al., 1994; Hampel et al., 2018), which makes the efflux of these chemically reduced N forms important for productivity and HABs in eutrophic systems (Glibert, 2017). NH_4^+ also increases the growth and toxicity of *Microcystis* (Donald et al., 2011; Monchamp et al., 2014; Gobler et al., 2016; Chaffin et al., 2018a), which cannot fix atmospheric N and is the main bloom-forming organism in western Lake Erie and many other eutrophic systems. Urea can be metabolized by cyanobacteria, including *Microcystis*, as a source of bioavailable N (Belisle et al., 2016) by hydrolysis to NH_4^+ within the cell (Mackerras and Smith, 1986). Both NH_4^+ and urea additions have stimulated increased chlorophyll-*a* concentrations in many eutrophic lakes (e.g., Donald et al., 2011), as well as higher microcystin production (Davis et al., 2015; Chaffin et al., 2018a). Overall, the

continuous flux of NH_4^+ and urea from the sediments may help explain why *Microcystis* remains dominant in Lake Erie during late summer, when ambient N concentrations are low and N-limited growth has been documented (Chaffin et al. 2014).

For DNRA, NIAF, as total NH_4^+ flux in $^{15}NO_3^-$ amended cores less total NH_4^+ flux in unamended cores (McCarthy et al. 2016), was used as a proxy. When observed as a positive value (15 of 32 incubations), NIAF accounted for, on average, ~80% of total NH_4^+ flux from sediments amended with $^{15}NO_3^-$, suggesting that DNRA could be active in western basin sediments (McCarthy et al., 2016). We could not confirm the importance of DNRA relative to denitrification or sediment NH_4^+ flux without isolating $^{15}NH_4^+$ from reduced organic N forms (e.g., by chromatography; Gardner et al., 2006; Lu et al., 2020).

Unlike NH_4^+ and urea, net NO_3^- flux was usually into sediments. Net NO_3^- uptake often occurred in conjunction with net *in situ* denitrification rates, indicating direct denitrification of NO_3^- from overlying water (Mulholland et al., 2008; Nogaro and Burgin, 2014). Net NO_3^- efflux, on the other hand, could indicate uncoupled nitrification – denitrification or nitrification exceeding denitrification. Net NO_2^- fluxes in unamended cores were relatively low, and there was no pattern in the flux direction (negative or positive). NO_2^- is an intermediate product of both nitrification and denitrification (Lomas and Lipschultz, 2006) and can be released or assimilated. However, NO_2^- is typically oxidized to NO_3^- or reduced to NO very quickly via nitrification and denitrification, respectively, due in part to its toxicity to many microbes (Stein and Arp, 1998).

We hypothesized that sediments would be a consistent source of ortho-P, and that was true for all but two sampling events (both in 2016 at WE13). Ortho-P was released despite the existence of oxic overlying water. Ortho-P release without hypoxic/anoxic bottom water is likely

explained by remineralization of organic matter, as both ortho-P ($\rho = 0.728$, $p < 0.001$) and NH_4^+ fluxes ($\rho = 0.792$, $p < 0.001$) were correlated with SOD and to one another ($\rho = 0.624$, $p < 0.001$; Figure 6; ESM Table S3). Lower microbial activity (e.g., remineralization) at WE13 could account for ortho-P influx observed in both early summer and fall. This site is farthest from the Maumee River discharge and exhibited lower SOD versus other sites (Figure 3). These results support those from other lakes, where ortho-P fluxes were lower in winter, presumably due to low biological activity (Holdren and Armstrong, 1980), and lower farthest from nutrient inputs (McCarthy et al., 2007; 2016). Ortho-P release from sediments can contribute to primary production and HABs, and *in situ* ortho-P fluxes in this study were comparable to those measured previously in Lake Erie (Matisoff et al., 2016) and elsewhere (McCarthy et al., 2007; McCarthy et al., 2016).

Sediment N_2 dynamics

Denitrification and anammox are key pathways to naturally reduce N over-enrichment in aquatic systems (Seitzinger, 1988), while N fixation provides new, bioavailable N (Schubert et al., 2006). Denitrification and anammox are beneficial ecosystem services because bioavailable N is reduced to N_2, which is then released to the atmosphere. All three processes occur simultaneously in sediments, and isotope additions can help disentangle these pathways in some cases. As hypothesized, possible anammox rates were always observed; however, the rates were low relative to denitrification (14% of potential denitrification rates), similar to results from Missisquoi Bay, Lake Champlain (8%; McCarthy et al., 2016). Possible anammox rates decreased with distance from the river mouth, although we cannot confirm anammox activity with the incubation approach used here, and abundance of the anammox-associated *hzo* gene,

encoding hydrazine oxidoreductase, was not quantified. Therefore, while measured net N_2 production includes denitrification and any anammox, we heretofore include any possible anammox when referring to denitrification.

The best estimates of *in situ* denitrification (i.e., net $^{28}N_2$ flux in unamended cores plus any calculated N fixation) were used from each sampling event to determine whether the sediments were providing an ecosystem service via N removal. Net N fixation was observed at WE4 in May 2016 and June 2017, MB18 in July 2016, and WE2 in April 2017. Net denitrification was observed at all other sites and times. This contrasts to our hypothesis that there would be net N fixation in the spring followed by net denitrification throughout the summer and fall. Denitrification is limited by NO_3^- and organic matter availability (Ward et al., 2009), and a pattern of early season net N fixation followed by net denitrification in the western basin suggested early season limitation by either NO_3^- or organic matter. However, with high spring discharges and NO_3^- loads entering Maumee Bay, it is more likely that organic matter was transported offshore and settled at sites farther from the river mouth, thus making organic matter the limiting factor of denitrification. The system then switched to net denitrification once there was sufficient labile organic matter. Future studies are needed to improve spatial and temporal resolution and attempt to constrain factors controlling the relative distributions of denitrification and N fixation in western Lake Erie and elsewhere.

Potential denitrification was calculated in the $^{15}NO_3^-$-amended cores to determine the capacity of sediments to conduct denitrification when NO_3^- was not limiting. Potential denitrification rates were higher in 2016 than 2017. Rates also peaked in mid-summer (July – August) at every site except WE4 in June 2016 and were similar to those measured in other freshwater systems using similar methods (e.g., McCarthy et al., 2007; Scott et al., 2008). Lower

ambient NO_3^- concentrations and N_2 effluxes in October of both 2016 and 2017 (when potential denitrification rates exceeded net *in situ* N_2 fluxes) reflect NO_3^- limitation of denitrification. During the rest of the year, however, potential denitrification and net *in situ* denitrification were not different (ANOVA; $p = 0.588$), suggesting that denitrifiers were not responsive to additional NO_3^- loads, and excess N from external loads was not being denitrified as efficiently. Sediment *nirS* gene copy abundance across all sites and sampling events was correlated with potential denitrification rates, confirming that increases in potential denitrification rates were accompanied by increased genetic potential.

Sediment N fixation by heterotrophic bacteria can occur regardless of bottom and porewater N concentrations (Knapp 2012; Newell et al., 2016) and may contribute to total N in aquatic systems. Positive N fixation rates were observed even when high DIN concentrations were present in the water column, supporting observations from other aquatic systems (Gardner et al., 2006; Fulweiler et al., 2007; Knapp, 2012; Foster and Fulweiler, 2014; Newell et al., 2016) and demonstrating that heterotrophic sediment N fixation is not necessarily sensitive to DIN concentrations. Calculated sediment N fixation rates were highest at MB18, which also tended to have the highest dissolved nutrient concentrations. N fixation rates and *nifH* gene abundance were only correlated at MB18 and WE2 ($\rho = 0.578$, $p = 0.019$).

Ability of western basin sediments to remove bioavailable N

Lake Erie is defined by three separate basins, and the western basin is the shallowest, warmest, and most productive (Ludsin et al., 2001). The western basin also exhibits the highest sedimentation rates due to high suspended solids loads from the Maumee and Detroit rivers (Kemp et al., 1977; Yuan et al., 2018). To scale measured N removal and N and P internal

loading rates for the entire western basin, each sampling site was designated to represent a specific section of the basin (ESM Figure S2). MB18 represented Maumee Bay, under direct influence of the river, and was the smallest, with an estimated surface area of 78 km^2, followed by WE2, with a surface area of 300 km^2, and WE4 and WE13 occupied the rest of the western basin with equal surface areas of 1301 km^2. Scaling results obtained from four locations within the entire basin is, of course, subject to uncertainties and assumes that these sampling locations are representative of the basin as a whole. For the rest of the basin (e.g., areas on the Canadian side, which were not available for sampling during this project), large deviations from rates measured at these four locations, occurring over very large areas of the basin, would affect the estimates presented and interpreted below. However, based on previous work on sediment accumulation in western Lake Erie (Kemp et al., 1977; Yuan et al., 2018), we believe that any such deviations would have relatively minor effects on results of the scaling exercise.

Overall, sediments were able to impact nutrient loads coming into the western basin. Combined total phosphorus (TP) loads into the western basin from the Maumee and Detroit Rivers were 4.26×10^6 kg P in 2016 and 5.74×10^6 kg P in 2017 (www.heidelberg.edu/academics/research-and-centers/national-center-for-water-quality-research). Scaled to the entire basin, sediments added 1.85×10^6 and 1.81×10^6 kg ortho-P in 2016 and 2017, respectively, which are equivalent to 43.5% and 31.5% of the TP load in these years, respectively. These estimates are similar to those comparing internal P loads in western Lake Erie to target P concentrations of 3.0 – 6.3 μg/L identified by the International Joint Commission for the western basin (20 – 42%; Matisoff et al., 2016).

The annual total nitrogen (TN) load entering the western basin from both rivers was 1.67×10^8 kg N in 2016 and 1.78×10^8 kg N in 2017 (www.heidelberg.edu/academics/research-and-

centers/national-center-for-water-quality-research). Sediments added NH_4^+ and urea to the water column at rates equivalent to 10.9% of the TN load in 2016 and 3.93% in 2017. However, they were a net sink for NO_x (NO_3^- + NO_2^-) and had a positive average release of N_2 gas, potentially removing 4.05×10^7 kg of bioavailable N in 2016 and 1.62×10^7 kg in 2017. Using our best estimate of *in situ* denitrification, and extrapolating to include estimated winter rates (estimated to be similar to summer rates; Cavaliere and Baulch, 2018), sediments removed an average of 34.9% of the TN load in 2016 and 13.4% of the TN load in 2017. These results show that higher N loads and lower residence times reduced the ability of Lake Erie sediments to remove bioavailable N in 2017. Other studies have also found that high external N loads inhibit denitrification efficiency in aquatic systems (Mulholland et al., 2008; Gardner and McCarthy, 2009). In less extensive bloom years (i.e., 2016), when N removal via denitrification was more efficient, internal recycling mechanisms were more important in providing bioavailable N and P to the water column (Table 4). Next research steps in western Lake Erie and other impacted systems could include incorporating these N cycling process rates into ecosystem models to better predict these ecosystem dynamics relative to changes in external nutrient loading and global climate change.

Conclusion

We quantified nutrient removal and recycling rates in the sediments at four sites in the western basin of Lake Erie (Figure 7). Sediments removed 34.9% and 13.4% of the external TN load in 2016 and 2017, respectively, via denitrification and, possibly, anammox. N fixation occurring simultaneously with denitrification in sediments was a source of bioavailable N from sediments throughout the study. As hypothesized, sediments were a net source of NH_4^+ (and

urea) and ortho-P, which can help sustain *Microcystis* blooms. Because this study was limited by the logistics of safely sampling during the winter and transitional seasons (e.g., early spring and late fall), sediment dynamics during ice-over have yet to be evaluated but are critical for quantifying annual sediment sinks and nutrient budgets. Emphasis should focus on best management practices to reduce non-point, agricultural sources of both N and P. High nutrient loads lead to larger HABs, both of which inhibit the efficiency of sediments in removing bioavailable N via denitrification and performing a valuable ecosystem service.

Acknowledgements

We thank Tom Bridgeman at the University of Toledo for assistance with boat time, Daniel Hoffman, Justyna Hampel, Megan Reed, and Justin Myers for their help in the lab and field, and Captain Craig Genheimer and staff at the OSU Stone Laboratory. We also thank the team at Heidelberg University National Center for Water Quality Research and David Fanslow (NOAA-GLERL, for providing phytoplankton community structure). This work was supported by Ohio Sea Grant R/ER-113 to MJM.

References

An, S., Gardner, W.S., Kana, T., 2001. Simultaneous Measurement of Denitrification and Nitrogen Fixation Using Isotope Pairing with Membrane Inlet Mass Spectrometry Analysis. Appl. Environ. Microbiol. 67, 1171–1178. https://doi.org/10.1128/AEM.67.3.1171-1178.2001

Baker, D.B., Confesor, R., Ewing, D.E., Johnson, L.T., Kramer, J.W., Merryfield, B.J., 2014. Phosphorus loading to Lake Erie from the Maumee, Sandusky and Cuyahoga rivers: The importance of bioavailability. J. Great Lakes Res. 40, 502–517. https://doi.org/10.1016/j.jglr.2014.05.001

Belisle, B.S., Steffen, M.M., Pound, H.L., Watson, S.B., DeBruyn, J.M., Bourbonniere, R.A.,

Boyer, G.L., Wilhelm, S.W., 2016. Urea in Lake Erie: Organic nutrient sources as potentially important drivers of phytoplankton biomass. J. Great Lakes Res. 42, 599–607. https://doi.org/10.1016/j.jglr.2016.03.002

Berman, T., Béchemin, C., Maestrini, S., 1999. Release of ammonium and urea from dissolved organic nitrogen in aquatic ecosystems. Aquat. Microb. Ecol. 16, 295–302. https://doi.org/10.3354/ame016295

Bernot, M.J., Dodds, W.K., Gardner, W.S., McCarthy, M.J., Sobolev, D., Tank, J.L., 2003. Comparing Denitrification Estimates for a Texas Estuary by Using Acetylene Inhibition and Membrane Inlet Mass Spectrometry. Applied and Environmental Microbiology 69, 5950–5956. https://doi.org/10.1128/AEM.69.10.5950-5956.2003

Blomqvist, P., Pettersson, A., Hyenstrand, P., 1994. Ammonium-nitrogen: A key regulatory factor causing dominance of non-nitrogen-fixing cyanobacteria in aquatic systems. Arch. Hydrobiol. 132, 141–164.

Bridgeman, T.B., Chaffin, J.D., Filbrun, J.E., 2013. A novel method for tracking western Lake Erie Microcystis blooms, 2002–2011. J. Great Lakes Res. 39, 83–89. https://doi.org/10.1016/j.jglr.2012.11.004

Brune, A., Frenzel, P., Cypionka, H., 2000. Life at the oxic–anoxic interface: microbial activities and adaptations. FEMS Microbiol Rev 24, 691–710. https://doi.org/10.1111/j.1574-6976.2000.tb00567.x

Carmichael, W.W., Boyer, G.L., 2016. Health impacts from cyanobacteria harmful algae blooms: Implications for the North American Great Lakes. Harmful Algae 54, 194–212. https://doi.org/10.1016/j.hal.2016.02.002

Carrick, H.J., Moon, J.B., Gaylord, B.F., 2005. Phytoplankton Dynamics and Hypoxia in Lake Erie: A Hypothesis Concerning Benthic-pelagic Coupling in the Central Basin. Journal of Great Lakes Research 31, 111–124. https://doi.org/10.1016/S0380-1330(05)70308-7

Cavaliere, E., Baulch, H.M., 2018. Denitrification under lake ice. Biogeochemistry 137, 285–295. https://doi.org/10.1007/s10533-018-0419-0

Chaffin, J.D., Bridgeman, T.B., Bade, D.L., Mobilian, C.N., 2014. Summer phytoplankton nutrient limitation in Maumee Bay of Lake Erie during high-flow and low-flow years. Journal of Great Lakes Research 40, 524–531. https://doi.org/10.1016/j.jglr.2014.04.009

Chaffin, J.D., Davis, T.W., Smith, D.J., Baer, M.M., Dick, G.J., 2018a. Interactions between

nitrogen form, loading rate, and light intensity on Microcystis and Planktothrix growth and microcystin production. Harmful Algae 73, 84–97. https://doi.org/10.1016/j.hal.2018.02.001

Chaffin, J.D., Kane, D.D., Stanislawczyk, K., Parker, E.M., 2018b. Accuracy of data buoys for measurement of cyanobacteria, chlorophyll, and turbidity in a large lake (Lake Erie, North America): implications for estimation of cyanobacterial bloom parameters from water quality sonde measurements. Environmental Science and Pollution Research 25, 25175–25189. https://doi.org/10.1007/s11356-018-2612-z

Clough, L.M., Renaud, P.E., Ambrose Jr., W.G., 2005. Impacts of water depth, sediment pigment concentration, and benthic macrofaunal biomass on sediment oxygen demand in the western Arctic Ocean. Can. J. Fish. Aquat. Sci. 62, 1756–1765. https://doi.org/10.1139/f05-102

Davis, T.W., Bullerjahn, G.S., Tuttle, T., McKay, R.M., Watson, S.B., 2015. Effects of Increasing Nitrogen and Phosphorus Concentrations on Phytoplankton Community Growth and Toxicity During *Planktothrix* Blooms in Sandusky Bay, Lake Erie. Environ. Sci. Technol. 49, 7197–7207. https://doi.org/10.1021/acs.est.5b00799

Donald, D.B., Bogard, M.J., Finlay, K., Leavitt, P.R., 2011. Comparative effects of urea, ammonium, and nitrate on phytoplankton abundance, community composition, and toxicity in hypereutrophic freshwaters. Limnol. Oceanogr. 56, 2161–2175. https://doi.org/10.4319/lo.2011.56.6.2161

Eyre, B.D., Rysgaard, S., Dalsgaard, T., Christensen, P.B., 2002. Comparison of Isotope Pairing and N2:Ar Methods for Measuring Sediment Denitrification—Assumptions, Modifications, and Implications. Estuaries 25, 1077–1087.

Forsberg, C., 1989. Importance of sediments in understanding nutrient cyclings in lakes. Hydrobiologia 176, 263–277.

Foster, S.Q., Fulweiler, R.W., 2014. Spatial and historic variability of benthic nitrogen cycling in an anthropogenically impacted estuary. Front. Mar. Sci. 1, 1–16. https://doi.org/10.3389/fmars.2014.00056

Fox and Weisberg (2019). An R Companion to Applied Regression, Third Edition. Thousand Oaks CA: Sage. URL: https://socialsciences.mcmaster.ca/jfox/Books/Companion/

Fulweiler, R.W., Nixon, S.W., Buckley, B.A., Granger, S.L., 2007. Reversal of the net dinitrogen

gas flux in coastal marine sediments. Nature 448, 180–182. https://doi.org/10.1038/nature05963

Gardner, W.S., Lee, G.F., 1975. The role of amino acids in the nitrogen cycle of Lake Mendota. Limnol. Oceanogr. 20, 379–388. https://doi.org/10.4319/lo.1975.20.3.0379

Gardner, W.S., McCarthy, M.J., 2009. Nitrogen dynamics at the sediment–water interface in shallow, sub-tropical Florida Bay: why denitrification efficiency may decrease with increased eutrophication. Biogeochemistry 95, 185–198. https://doi.org/10.1007/s10533-009-9329-5

Gardner, W.S., McCarthy, M.J., An, S., Sobolev, D., Sell, K.S., Brock, D., 2006. Nitrogen fixation and dissimilatory nitrate reduction to ammonium (DNRA) support nitrogen dynamics in Texas estuaries. Limnol. Oceanogr. 51, 558–568. https://doi.org/10.4319/lo.2006.51.1_part_2.0558

Gardner, W.S., McCarthy, M.J., Carini, S.A., Souza, A.C., Lijun, H., McNeal, K.S., Puckett, M.K., Pennington, J., 2009. Collection of intact sediment cores with overlying water to study nitrogen- and oxygen-dynamics in regions with seasonal hypoxia. Cont. Shelf Res. 29, 2207–2213. https://doi.org/10.1016/j.csr.2009.08.012

Glibert, P.M., 2017. Eutrophication, harmful algae and biodiversity — Challenging paradigms in a world of complex nutrient changes. Marine Pollution Bulletin 124, 591–606. https://doi.org/10.1016/j.marpolbul.2017.04.027

Glibert, P.M., Harrison, J., Heil, C., Seitzinger, S., 2006. Escalating Worldwide use of Urea – A Global Change Contributing to Coastal Eutrophication. Biogeochemistry 77, 441–463. https://doi.org/10.1007/s10533-005-3070-5

Glibert, P.M., Hinkle, D.C., Sturgis, B., Jesien, R.V., 2014. Eutrophication of a Maryland/Virginia Coastal Lagoon: a Tipping Point, Ecosystem Changes, and Potential Causes. Estuar. Coast. 37, 128–146. https://doi.org/10.1007/s12237-013-9630-3

Glibert, P.M., Wilkerson, F.P., Dugdale, R.C., Raven, J.A., Dupont, C.L., Leavitt, P.R., Parker, A.E., Burkholder, J.M., Kana, T.M., 2016. Pluses and minuses of ammonium and nitrate uptake and assimilation by phytoplankton and implications for productivity and community composition, with emphasis on nitrogen-enriched conditions. Limnol. Oceanogr. 61, 165–197. https://doi.org/10.1002/lno.10203

Gobler, C.J., Burkholder, J.M., Davis, T.W., Harke, M.J., Johengen, T., Stow, C.A., Van de

Waal, D.B., 2016. The dual role of nitrogen supply in controlling the growth and toxicity of cyanobacterial blooms. Harmful Algae 54, 87–97. https://doi.org/10.1016/j.hal.2016.01.010

Hampel, J.J., McCarthy, M.J., Gardner, W.S., Zhang, L., Xu, H., Zhu, G., Newell, S.E., 2018. Nitrification and ammonium dynamics in Taihu Lake, China: seasonal competition for ammonium between nitrifiers and cyanobacteria. Biogeosciences 15, 733–748. https://doi.org/10.5194/bg-15-733-2018

Han, H., Allan, J.D., Bosch, N.S., 2012. Historical pattern of phosphorus loading to Lake Erie watersheds. J. Great Lakes Res. 38, 289–298. https://doi.org/10.1016/j.jglr.2012.03.004

Heisler, J., Glibert, P.M., Burkholder, J.M., Anderson, D.M., Cochlan, W., Dennison, W.C., Dortch, Q., Gobler, C.J., Heil, C.A., Humphries, E., Lewitus, A., Magnien, R., Marshall, H.G., Sellner, K., Stockwell, D.A., Stoecker, D.K., Suddleson, M., 2008. Eutrophication and harmful algal blooms: A scientific consensus. Harmful Algae 8, 3–13. https://doi.org/10.1016/j.hal.2008.08.006

Herrero, A., Muro-Pastor, A.M., Flores, E., 2001. Nitrogen Control in Cyanobacteria. Journal of Bacteriology 183, 411–425. https://doi.org/10.1128/JB.183.2.411-425.2001

Hoffman, D.K., McCarthy, M.J., Newell, S.E., Gardner, W.S., Niewinski, D.N., Gao, J., Mutchler, T.R., 2019. Relative Contributions of DNRA and Denitrification to Nitrate Reduction in Thalassia testudinum Seagrass Beds in Coastal Florida (USA). Estuaries and Coasts 42, 1001–1014. https://doi.org/10.1007/s12237-019-00540-2

Holdren, G.C., Armstrong, D.E., 1980. Factors affecting phosphorus release from intact lake sediment cores. Environ. Sci. Technol. 14, 79–87. https://doi.org/10.1021/es60161a014

Kana, T.M., Darkangelo, C., Hunt, M.D., Oldham, J.B., Bennett, G.E., Cornwell, J.C., 1994. Membrane lnlet Mass Spectrometer for Rapid High-Precision Determination of N2, O2 , and Ar in Environmental Water Samples. Anal. Chem. 66, 4166–4170.

Kana, T.M., Weiss, D.L., 2004. Comment on “Comparison of isotope pairing and N2:Ar methods for measuring sediment denitrification” by B. D. Eyre, S. Rysgaard, T. Dalsgaard, and P. Bondo Christensen. 2002.Estuaries 25:1077–1087. Estuaries 27, 173–176. https://doi.org/10.1007/BF02803571

Kane, D.D., Conroy, J.D., Peter Richards, R., Baker, D.B., Culver, D.A., 2014. Re-

eutrophication of Lake Erie: Correlations between tributary nutrient loads and phytoplankton biomass. J. Great Lakes Res. 40, 496–501. https://doi.org/10.1016/j.jglr.2014.04.004

Kassambara, A., 2018. ggpubr: 'ggplot2' based publication ready plots. R package version 0.2. https://CRAN.R-project.org/package=ggpubr

Kemp, A.L.W., MacInnis, G.A., Harper, N.S., 1977. Sedimentation Rates and a Revised Sediment Budget for Lake Erie. Journal of Great Lakes Research 3, 221–233. https://doi.org/10.1016/S0380-1330(77)72253-1

Knapp, A.N., 2012. The sensitivity of marine N2 fixation to dissolved inorganic nitrogen. Front. Microbiol. 3, 1–14. https://doi.org/10.3389/fmicb.2012.00374

Lavrentyev, P.J., Gardner, W.S., Yang, L., 2000. Effects of the zebra mussel on nitrogen dynamics and the microbial community at the sediment-water interface. Aquat. Microb. Ecol. 21, 187–194. https://doi.org/10.3354/ame021187

Lomas, M.W., Lipschultz, F., 2006. Forming the primary nitrite maximum: Nitrifiers or phytoplankton? Limnol. Oceanogr. 51, 2453–2467. https://doi.org/10.4319/lo.2006.51.5.2453

Lu, K., Lin, X., Gardner, W.S., Liu, Z., 2020. A streamlined method to quantify the fates of ^{15} N In seawater samples amended with ^{15} N-labeled organic nitrogen. Limnol Oceanogr Methods 18, 52–62. https://doi.org/10.1002/lom3.10345

Ludsin, S.A., Kershner, M.W., Blocksom, K.A., Knight, R.L., Stein, R.A., 2001. Life after death in Lake Erie: Nutrient controls drive fish species richness, rehabilitation. Ecol. Appl. 11, 731–746. https://doi.org/10.1890/1051-0761(2001)011[0731:LADILE]2.0.CO;2

Mackerras, A., H., Smith, G.D., 1986. Urease Activity of the Cyanobacterium *Anabaena cylindrica*. J. Gen. Microbiol. 132, 2749–2752.

Matisoff, G., Kaltenberg, E.M., Steely, R.L., Hummel, S.K., Seo, J., Gibbons, K.J., Bridgeman, T.B., Seo, Y., Behbahani, M., James, W.F., Johnson, L.T., Doan, P., Dittrich, M., Evans, M.A., Chaffin, J.D., 2016. Internal loading of phosphorus in western Lake Erie. J. Great Lakes Res. 42, 775–788. https://doi.org/10.1016/j.jglr.2016.04.004

McCarthy, M.J., Gardner, W.S., Lavrentyev, P.J., Moats, K.M., Jochem, F.J., Klarer, D.M., 2007. Effects of Hydrological Flow Regime on Sediment-water Interface and Water Column Nitrogen Dynamics in a Great Lakes Coastal Wetland (Old Woman Creek, Lake

Erie). J. Great Lakes Res. 33, 219–231. https://doi.org/10.3394/0380-1330(2007)33[219:EOHFRO]2.0.CO;2

McCarthy, M.J., James, R.T., Chen, Y., East, T.L., Gardner, W.S., 2009. Nutrient ratios and phytoplankton community structure in the large, shallow, eutrophic, subtropical Lakes Okeechobee (Florida, USA) and Taihu (China). Limnology 10, 215–227. https://doi.org/10.1007/s10201-009-0277-5

McCarthy, M.J., Newell, S.E., Carini, S.A., Gardner, W.S., 2015. Denitrification Dominates Sediment Nitrogen Removal and Is Enhanced by Bottom-Water Hypoxia in the Northern Gulf of Mexico. Estuar. Coast. 38, 2279–2294. https://doi.org/10.1007/s12237-015-9964-0

McCarthy, M.J., Gardner, W.S., Lehmann, M.F., Guindon, A., Bird, D.F., 2016. Benthic nitrogen regeneration, fixation, and denitrification in a temperate, eutrophic lake: Effects on the nitrogen budget and cyanobacteria blooms: Sediment N cycling in Missisquoi Bay. Limnology and Oceanography 61, 1406–1423. https://doi.org/10.1002/lno.10306

McTigue, N.D., Gardner, W.S., Dunton, K.H., Hardison, A.K., 2016. Biotic and abiotic controls on co-occurring nitrogen cycling processes in shallow Arctic shelf sediments. Nat. Commun. 7, 13145. https://doi.org/10.1038/ncomms13145

Michalak, A.M., Anderson, E.J., Beletsky, D., Boland, S., Bosch, N.S., Bridgeman, T.B., Chaffin, J.D., Cho, K., Confesor, R., Daloglu, I., DePinto, J.V., Evans, M.A., Fahnenstiel, G.L., He, L., Ho, J.C., Jenkins, L., Johengen, T.H., Kuo, K.C., LaPorte, E., Liu, X., McWilliams, M.R., Moore, M.R., Posselt, D.J., Richards, R.P., Scavia, D., Steiner, A.L., Verhamme, E., Wright, D.M., Zagorski, M.A., 2013. Record-setting algal bloom in Lake Erie caused by agricultural and meteorological trends consistent with expected future conditions. Proc. Natl. Acad. Sci. 110, 6448–6452. https://doi.org/10.1073/pnas.1216006110

Monchamp, M.-E., Pick, F.R., Beisner, B.E., Maranger, R., 2014. Nitrogen Forms Influence Microcystin Concentration and Composition via Changes in Cyanobacterial Community Structure. PLoS ONE 9. https://doi.org/10.1371/journal.pone.0085573

Moog, D.B., Whiting, P.J., 2002. Climatic and Agricultural Factors in Nutrient Exports from Two Watersheds in Ohio. J. Environ. Qual. 31, 12.

Mulholland, P.J., Helton, A.M., Poole, G.C., Hall, R.O., Hamilton, S.K., Peterson, B.J., Tank,

J.L., Ashkenas, L.R., Cooper, L.W., Dahm, C.N., Dodds, W.K., Findlay, S.E.G., Gregory, S.V., Grimm, N.B., Johnson, S.L., McDowell, W.H., Meyer, J.L., Valett, H.M., Webster, J.R., Arango, C.P., Beaulieu, J.J., Bernot, M.J., Burgin, A.J., Crenshaw, C.L., Johnson, L.T., Niederlehner, B.R., O'Brien, J.M., Potter, J.D., Sheibley, R.W., Sobota, D.J., Thomas, S.M., 2008. Stream denitrification across biomes and its response to anthropogenic nitrate loading. Nature 452, 202–205. https://doi.org/10.1038/nature06686

Murphy, T., Irvine, K., Guo, J., Davies, J., Murkin, H., Charlton, M., Watson, S., 2003. New Microcystin Concerns in the Lower Great Lakes. Water Qual. Res. J. Canada 38, 127–140. https://doi.org/10.2166/wqrj.2003.008

Newell, S.E., Davis, T.W., Johengen, T.H., Gossiaux, D., Burtner, A., Palladino, D., McCarthy, M.J., 2019. Reduced forms of nitrogen are a driver of non-nitrogen-fixing harmful cyanobacterial blooms and toxicity in Lake Erie. Harmful Algae 81, 86–93. https://doi.org/10.1016/j.hal.2018.11.003

Newell, S.E., McCarthy, M.J., Gardner, W.S., Fulweiler, R.W., 2016. Sediment Nitrogen Fixation: a Call for Re-evaluating Coastal N Budgets. Estuar. Coast. 39, 1626–1638. https://doi.org/10.1007/s12237-016-0116-y

Nielsen, L.P., 1992. Denitrification in sediment determined from nitrogen isotope pairing. FEMS Microbiology Ecology 86, 357–362.

Nogaro, G., Burgin, A.J., 2014. Influence of bioturbation on denitrification and dissimilatory nitrate reduction to ammonium (DNRA) in freshwater sediments. Biogeochemistry 120, 279–294. https://doi.org/10.1007/s10533-014-9995-9

Ohio Environmental Protection Agency, Department of Surface Water Modeling and Assessment Section. (2018). *Nutrient Mass Balance Study for Ohio's Major Rivers.* Retrieved from https://epa.ohio.gov/Portals/35/documents/Nutrient%20Mass%20Balance%20Study%202018_Final.pdf

Paerl, H.W., Otten, T.G., 2013. Harmful Cyanobacterial Blooms: Causes, Consequences, and Controls. Microb. Ecol. 65, 995–1010. https://doi.org/10.1007/s00248-012-0159-y

Paerl, H.W., Scott, J.T., McCarthy, M.J., Newell, S.E., Gardner, W.S., Havens, K.E., Hoffman, D.K., Wilhelm, S.W., Wurtsbaugh, W.A., 2016. It Takes Two to Tango: When and Where Dual Nutrient (N & P) Reductions Are Needed to Protect Lakes and Downstream Ecosystems. Environ. Sci. Technol. 50, 10805–10813. https://doi.org/10.1021/acs.est.6b02575

Paytan, A., Roberts, K., Watson, S., Peek, S., Chuang, P.-C., Defforey, D., Kendall, C., 2017. Internal loading of phosphate in Lake Erie Central Basin. Sci. Total Environ. 579, 1356–1365. https://doi.org/10.1016/j.scitotenv.2016.11.133

R Core Team, 2019. R: A language and environment for statistical computing., Vienna, Austria. https://www.R-project.org/

Richards, R.P., Baker, D.B., Crumrine, J.P., Stearns, A.M., 2010. Unusually large loads in 2007 from the Maumee and Sandusky Rivers, tributaries to Lake Erie. J. Soil Water Conserv. 65, 450–462. https://doi.org/10.2489/jswc.65.6.450

Romo, S., Soria, J., Fernández, F., Ouahid, Y., Barón-Solá, Á., 2013. Water residence time and the dynamics of toxic cyanobacteria: *Water residence time and toxic cyanobacteria*. Freshwater Biology 58, 513–522. https://doi.org/10.1111/j.1365-2427.2012.02734.x

Salk, K.R., Bullerjahn, G.S., McKay, R.M.L., Chaffin, J.D., Ostrom, N.E., 2018. Nitrogen cycling in Sandusky Bay, Lake Erie: oscillations between strong and weak export and implications for harmful algal blooms. Biogeosciences 15, 2891–2907. https://doi.org/10.5194/bg-15-2891-2018

Schubert, C.J., Durisch-Kaiser, E., Wehrli, B., Thamdrup, B., Lam, P., Kuypers, M.M.M., 2006. Anaerobic ammonium oxidation in a tropical freshwater system (Lake Tanganyika). Environ. Microbiol. 8, 1857–1863. https://doi.org/10.1111/j.1462-2920.2006.01074.x

Scott, J.T., McCarthy, M.J., Gardner, W.S., Doyle, R.D., 2008. Denitrification, dissimilatory nitrate reduction to ammonium, and nitrogen fixation along a nitrate concentration gradient in a created freshwater wetland. Biogeochemistry 87, 99–111. https://doi.org/10.1007/s10533-007-9171-6

Seiki, T., Izawa, H., Date, E., Sunahara, H., 1994. Sediment oxygen demand in Hiroshima Bay. Water Res. 28, 385–393. https://doi.org/10.1016/0043-1354(94)90276-3

Seitzinger, S.P., 1988. Denitrification in freshwater and coastal marine ecosystems: Ecological and geochemical significance. Limnol. Oceanogr. 33, 702–724. https://doi.org/10.4319/lo.1988.33.4part2.0702

Small, G.E., Cotner, J.B., Finlay, J.C., Stark, R.A., Sterner, R.W., 2014. Nitrogen transformations at the sediment–water interface across redox gradients in the Laurentian Great Lakes. Hydrobiologia 731, 95–108. https://doi.org/10.1007/s10750-013-1569-7

Smetacek, V.S., 1985. Role of sinking in diatom life-history cycles: ecological, evolutionary and geological significance. Mar. Biol. 84, 239–251. https://doi.org/10.1007/BF00392493

Steffen, M.M., Belisle, B.S., Watson, S.B., Boyer, G.L., Wilhelm, S.W., 2014. Status, causes and ontrols of cyanobacterial blooms in Lake Erie. J. Great Lakes Res. 40, 215–225. https://doi.org/10.1016/j.jglr.2013.12.012

Stein, L.Y., Arp, D.J., 1998. Loss of Ammonia Monooxygenase Activity in *Nitrosomonas europaea* upon Exposure to Nitrite. Appl. Environ. Microbiol. 64, 4098–4102.

Stow, C.A., Cha, Y., Johnson, L.T., Confesor, R., Richards, R.P., 2015. Long-Term and Seasonal Trend Decomposition of Maumee River Nutrient Inputs to Western Lake Erie. Environ. Sci. Technol. 49, 3392–3400. https://doi.org/10.1021/es5062648

Stumpf, R.P., Wynne, T.T., Baker, D.B., Fahnenstiel, G.L., 2012. Interannual Variability of Cyanobacterial Blooms in Lake Erie. PLoS ONE 7, e42444. https://doi.org/10.1371/journal.pone.0042444

Verhamme, E.M., Redder, T.M., Schlea, D.A., Grush, J., Bratton, J.F., DePinto, J.V., 2016. Development of the Western Lake Erie Ecosystem Model (WLEEM): Application to connect phosphorus loads to cyanobacteria biomass. J. Great Lakes Res. 42, 1193–1205. https://doi.org/10.1016/j.jglr.2016.09.006

Ward, B.B., Devol, A.H., Rich, J.J., Chang, B.X., Bulow, S.E., Naik, H., Pratihary, A., Jayakumar, A., 2009. Denitrification as the dominant nitrogen loss process in the Arabian Sea. Nature 461, 78–81. https://doi.org/10.1038/nature08276

Watson, S.B., Miller, C., Arhonditsis, G., Boyer, G.L., Carmichael, W., Charlton, M.N., Confesor, R., Depew, D.C., Höök, T.O., Ludsin, S.A., Matisoff, G., McElmurry, S.P., Murray, M.W., Peter Richards, R., Rao, Y.R., Steffen, M.M., Wilhelm, S.W., 2016. The re-eutrophication of Lake Erie: Harmful algal blooms and hypoxia. Harmful Algae 56, 44–66. https://doi.org/10.1016/j.hal.2016.04.010

Wilson, T., DePaul, V., 2017. *In Situ* Benthic Nutrient Flux and Sediment Oxygen Demand in Barnegat Bay, New Jersey. J. Coast. Res. 78, 46–59. https://doi.org/10.2112/SI78-005.1

Yuan, F., Chaffin, J.D., Xue, B., Wattrus, N., Zhu, Y., Sun, Y., 2018. Contrasting sources and mobility of trace metals in recent sediments of western Lake Erie. Journal of Great Lakes Research 44, 1026–1034. https://doi.org/10.1016/j.jglr.2018.07.016

Tables

Table 1: Surface and bottom water sonde data from each sampling date and site. Temperature is in degrees Celsius, dissolved oxygen is in mg/L, and chl-*a* fluorescence is reported as µg/L.

		Surface Water			Bottom Water		
Site	Date	Temperature	DO	Chl-a	Temperature	DO	Chl-a
MB18	7/13/2016	25.1	8.65	13.4	25.1	8.65	13.4
	8/3/2016	27.2	10.7	2.91	26.8	9.27	3.52
	9/19/2016	21.8	8.33	8.84	21.7	8.23	8.84
	10/17/2016	16.5	9.12	ND	16.5	9.09	0.43
	4/25/2017	14.0	10.5	6.68	14.0	10.0	7.52
	7/11/2017	26.3	8.65	12.6	23.6	7.04	3.40
	8/9/2017	24.0	9.18	4.19	23.0	8.55	3.59
	10/3/2017	18.5	9.58	7.36	18.5	9.51	9.43
WE2	7/13/2016	25.1	8.32	3.58	24.9	8.21	1.86
	8/3/2016	26.6	9.68	3.34	25.7	6.32	1.23
	9/19/2016	22.1	7.88	1.92	21.9	7.35	0.53
	10/17/2016	16.9	9.24	0.55	16.9	9.23	0.56
	4/25/2017	11.8	11.3	13.6	11.8	11.4	10.1
	7/11/2017	26.1	8.29	1.05	22.8	7.81	1.18
	8/9/2017	23.9	5.74	0.16	23.0	8.23	0.22
	10/3/2017	19.7	9.62	3.27	19.8	8.81	3.52
WE4	5/18/2016	12.1	10.9	0.85	12.1	10.8	2.62
	6/28/2016	24.2	8.83	1.25	23.3	9.33	0.35
	8/10/2016	26.6	8.02	3.01	25.7	8.53	2.92
	10/3/2016	18.2	8.94	1.58	18.1	8.78	0.16
	6/9/2017	17.9	9.71	0.84	17.6	9.94	1.15
	7/14/2017	23.7	8.57	2.43	23.6	8.28	1.85
	8/2/2017	24.0	9.18	4.19	24.2	5.89	0.20
	10/20/2017	16.1	10.1	0.88	16.1	9.91	1.44
WE13	5/18/2016	12.0	11.1	1.65	11.9	11.1	4.78
	6/28/2016	23.8	6.67	0.77	22.8	6.77	3.61
	8/10/2016	26.2	8.13	8.44	25.9	8.36	7.19
	10/3/2016	18.8	8.72	1.83	18.8	8.72	0.28
	6/9/2017	18.9	9.64	1.03	18.2	9.53	1.70
	7/14/2017	23.2	8.64	2.03	23.2	8.40	2.14
	8/2/2017	25.4	8.90	0.82	23.8	6.01	0.12
	10/20/2017	16.7	9.97	2.88	16.7	9.60	5.41

Table 2: Dissolved water column nutrient concentrations at each sampling site and time. Units are in µM N or P. Measurements below the detection limit are reported as BDL.

		Surface Water					Bottom Water				
Site	Date	NH_4^+	NO_2^-	NO_3^-	Urea	Ortho-P	NH_4^+	NO_2^-	NO_3^-	Urea	Ortho-P
MB18	7/13/2016	0.20	1.38	53.4	6.20	0.20	2.53	1.42	58.0	1.43	0.14
	8/3/2016	5.95	2.92	50.3	0.28	0.05	2.92	1.52	66.1	1.24	0.07
	9/19/2016	0.49	0.780	9.84	1.30	0.63	0.80	0.57	9.99	2.15	0.79
	10/17/2016	2.06	0.65	27.4	1.05	0.74	1.87	0.74	30.0	1.21	0.80
	4/25/2017	4.60	3.08	228	3.51	1.35	4.60	3.22	241	4.28	1.17
	7/11/2017	7.24	11.2	487	4.95	1.76	7.27	10.8	481	3.71	1.94
	8/9/2017	1.12	1.35	98.7	1.39	0.22	1.41	1.26	97.0	6.18	0.20
	10/3/2017	BDL	0.08	0.01	0.67	0.09	BDL	0.03	0.08	0.53	0.18
WE2	7/13/2016	0.09	1.44	17.7	4.03	0.09	1.84	0.80	38.4	1.71	0.09
	8/3/2016	0.28	1.61	4.01	1.47	0.05	1.61	0.49	12.2	1.37	0.05
	9/19/2016	2.41	7.87	5.78	1.57	0.89	7.87	0.75	5.68	1.13	0.94
	10/17/2016	0.43	0.74	20.0	0.73	0.38	0.23	0.75	20.4	0.45	0.38
	4/25/2017	3.81	0.75	60.0	2.07	0.10	3.59	0.67	58.5	1.53	0.05
	7/11/2017	1.17	0.68	51.9	1.93	0.10	2.80	0.75	46.5	1.78	0.16
	8/9/2017	1.03	0.74	34.8	3.58	0.04	1.11	0.71	34.6	2.00	0.06
	10/3/2017	0.83	0.65	14.5	0.95	0.13	0.69	0.61	14.6	0.86	0.12
WE4	5/18/2016	0.83	7.29	6.75	0.44	0.06	1.72	7.29	9.46	0.59	0.05
	6/28/2016	1.58	1.02	23.3	2.42	0.03	1.02	0.64	23.1	0.61	0.03
	8/10/2016	3.20	1.94	8.85	1.15	0.05	1.94	0.79	10.2	2.13	0.08
	10/3/2016	1.86	0.43	18.9	0.94	0.57	1.90	0.43	18.8	0.78	0.56
	6/9/2017	0.30	0.31	31.0	0.70	0.01	0.84	0.29	31.3	1.04	0.03
	7/14/2017	1.21	1.19	37.9	1.17	0.03	1.40	0.82	37.5	0.93	0.03
	8/2/2017	0.99	2.25	93.8	0.93	0.03	0.26	2.37	90.2	1.33	0.04
	10/20/2017	0.41	0.17	14.8	0.33	0.09	0.32	0.17	14.8	0.29	0.09
WE13	5/18/2016	0.29	7.29	19.7	0.28	0.05	6.04	7.28	15.5	0.41	0.06
	6/28/2016	0.28	0.42	21.9	1.01	0.03	0.42	1.22	27.1	1.27	0.03
	8/10/2016	0.20	0.84	1.62	3.23	0.07	0.84	0.23	2.75	1.27	0.07
	10/3/2016	0.95	2.56	7.83	1.12	1.13	0.91	2.53	7.81	1.21	1.13
	6/9/2017	1.91	0.45	33.1	0.88	0.01	2.88	0.45	33.3	4.40	0.06
	7/14/2017	1.19	0.98	34.7	0.53	0.05	0.56	0.36	34.8	0.71	0.03
	8/2/2017	BDL	0.61	41.0	0.30	0.04	0.28	0.53	35.3	0.71	0.04
	10/20/2017	0.53	0.34	14.6	0.43	0.36	0.47	0.34	14.2	0.42	0.37

Table 3: Dissolved water column N and ortho-P fluxes from duplicate unamended cores. A positive value indicates an efflux from the sediment, and a negative value shows influx into the sediment. SE indicates standard error. Units are in μmol N (or P)/m^2/hr.

Site	Date	NH_4^+	SE	NO_2^-	SE	NO_3^-	SE	Urea	SE	Ortho-P	SE
MB18	7/13/16	55.9	20.1	-7.52	3.90	-114	42.4	2.37	2.37	4.37	0.44
	8/3/16	58.6	11.1	-1.71	1.74	-205	69.7	5.73	3.15	1.28	0.48
	9/19/16	154	22.1	0.42	1.09	5.70	10.3	2.77	4.61	5.85	0.78
	10/17/16	119	22.0	8.12	2.96	-53.0	23.8	15.4	2.11	6.17	1.22
	4/25/17	66.1	17.1	-11.7	5.85	-46.7	75.6	9.47	3.78	9.36	1.89
	7/11/17	79.4	33.2	-31.5	11.5	-222	117	26.5	7.13	13.0	2.06
	8/9/17	34.6	3.88	-1.80	2.05	-143	49.9	4.34	2.01	2.93	0.22
	10/3/17	4.82	2.67	3.04	1.35	22.4	7.42	2.50	1.22	1.80	0.49
WE2	7/13/16	-6.99	12.8	-1.58	0.75	9.53	18.4	-4.44	5.36	2.47	0.62
	8/3/16	32.5	9.29	-0.30	0.21	-26.8	6.36	10.7	5.79	1.20	0.27
	9/19/16	52.7	20.4	-2.57	0.90	-17.8	7.28	12.9	3.70	2.31	0.95
	10/17/16	-13.1	2.43	0.69	1.56	14.6	15.2	-2.64	2.43	2.13	0.51
	4/25/17	-10.6	3.91	-1.67	0.27	12.4	17.7	4.83	5.69	0.56	0.32
	7/11/17	16.2	7.67	3.74	1.69	-49.1	23.2	18.8	3.27	0.31	0.07
	8/9/17	-5.25	1.24	4.17	1.17	-22.2	5.42	1.62	1.93	0.53	0.06
	10/3/17	5.37	2.70	-3.39	1.11	-4.11	2.05	-0.10	0.83	0.47	0.08
WE4	5/18/16	6.99	2.50	-0.07	0.32	-21.6	3.84	-0.42	0.64	0.71	0.11
	6/28/16	34.0	14.4	-2.26	1.88	-18.0	35.5	-0.22	2.65	3.00	0.94
	8/10/16	42.4	7.68	-2.37	0.39	21.1	1.40	2.58	2.06	1.56	0.34
	10/3/16	117	23.4	2.59	2.76	-79.4	67.8	8.88	1.63	4.47	1.24
	6/9/17	2.95	1.92	0.25	0.11	-5.77	13.4	-3.09	2.37	0.19	0.11
	7/14/17	5.95	3.63	-5.81	1.25	-19.8	4.05	7.90	2.44	0.06	0.10
	8/2/17	-12.9	6.90	0.28	2.71	-115	34.9	6.43	3.89	0.61	0.07
	10/20/17	34.8	10.6	4.91	1.14	8.31	10.9	9.12	1.58	2.37	0.63
WE13	5/18/16	52.9	24.3	3.10	2.06	-22.7	2.36	1.96	0.25	0.68	0.18
	6/28/16	11.0	2.93	0.11	0.24	-15.7	13.3	5.49	3.48	-0.27	0.49
	8/10/16	7.35	2.31	-0.40	0.19	12.6	10.9	2.54	2.51	0.48	0.13
	10/3/16	5.98	2.08	-10.8	1.46	-0.89	12.8	-0.33	4.22	-1.01	0.92
	6/9/17	-11.9	1.55	0.03	0.20	5.38	19.0	-2.36	0.92	0.68	0.35
	7/14/17	-7.15	2.28	3.19	1.06	12.6	7.96	8.50	4.85	0.14	0.16
	8/2/17	-2.14	1.36	-0.97	2.68	-25.8	28.3	4.07	1.43	0.24	0.12
	10/20/17	11.7	3.67	-1.60	0.86	-9.63	5.65	-3.61	0.94	1.51	0.22

Table 4: Preliminary N budget for the western basin of Lake Erie. Units are in 10^6 kg N/yr. Estimated surface areas for extrapolations: MB18 = 78 km^2; WE2 = 300 km^2; WE4 and WE13 = 1301 km^2. DNF = denitrification, DIN = dissolved inorganic N (NH_4^++NO_2^-+NO_3^-), TN = total N, and WB = western basin. Positive rates indicate a net efflux from the sediment, and negative rates show a net influx into the sediment. These values were scaled to include the entire surface area of the western basin.

	Yearly Average		Average by Site			
	2016	2017	MB18	WE2	WE4	WE13
In Situ DNF	-58.3	-22.3	-0.850	-2.06	-25.4	-21.9
DIN Flux	16.3	3.96	0.633	0.322	4.55	1.20
Urea Flux	1.45	2.17	0.083	0.119	0.622	0.324
Total	-40.5	-16.2	-0.134	-1.62	-20.2	-20.4
TN Load to WB	167	178	3.66	14.1	61.0	61.0
N surplus	126	162	3.53	12.5	40.8	40.6

Figure Captions

Figure 1: Map showing sampling locations in the western basin of Lake Erie. Thin lines in the lake are international and state boundaries.

Figure 2: N transformations across the sediment-water interface at each site in the western basin of Lake Erie. A positive bar indicates efflux, and a negative bar shows influx. Error bars indicate one standard error.

Figure 3: Sediment oxygen demand (SOD) in the western basin. Error bars indicate one standard error.

Figure 4: N_2 transformations across the sediment-water interface in the western basin of Lake Erie: (A) in-situ N_2 flux ($^{28}N_2$ fluxes + any N fixation), (B) potential denitrification ($^{28}N_2$ + $^{29}N_2$ + $^{30}N_2$ + any N fixation), and (C) calculated N fixation. Isotope additions were not performed at WE4 on October 20, 2017.

Figure 5: Western basin gene abundance measured in gene copies per gram of wet sediment. *nirS* (A) codes for the nitrite reductase gene in denitrification, and *nifH* (B) codes for the nitrogenase gene in N fixation.

Figure 6: Linear correlations between (A) NH_4^+ fluxes and SOD, (B) ortho-P fluxes and SOD, and (C) ortho-P fluxes and NH_4^+ fluxes.

Figure 7: Conceptual model showing N and ortho-P cycling rates in 2016 and 2017. Rates are reported in µmol N, P, or O_2/m^2/hr. DNRA was estimated using NIAF as a proxy, as explained in methods, and SOD was used as a proxy for organic matter remineralization.

Figure 1:

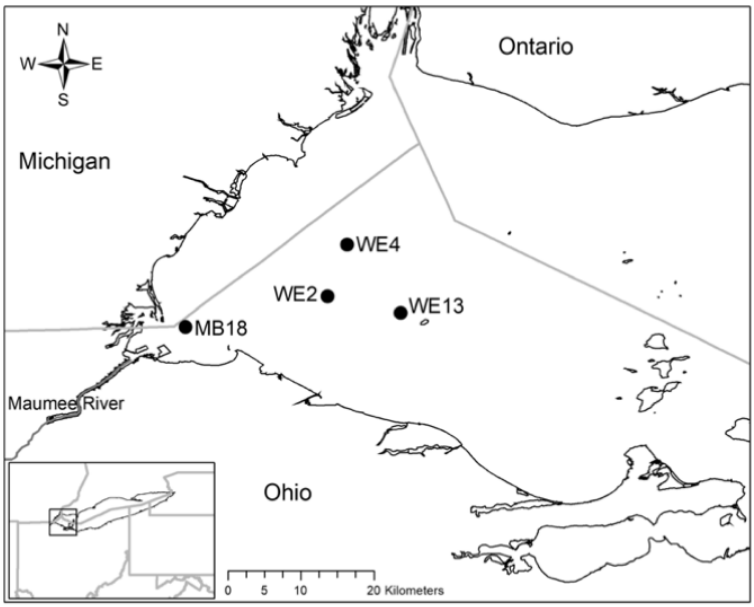
N
W
E
S
Ontario
Michigan
WE4
WE2
WE13
MB18
Maumee River
Ohio
0 5 10 20 Kilometers

Figure 2:

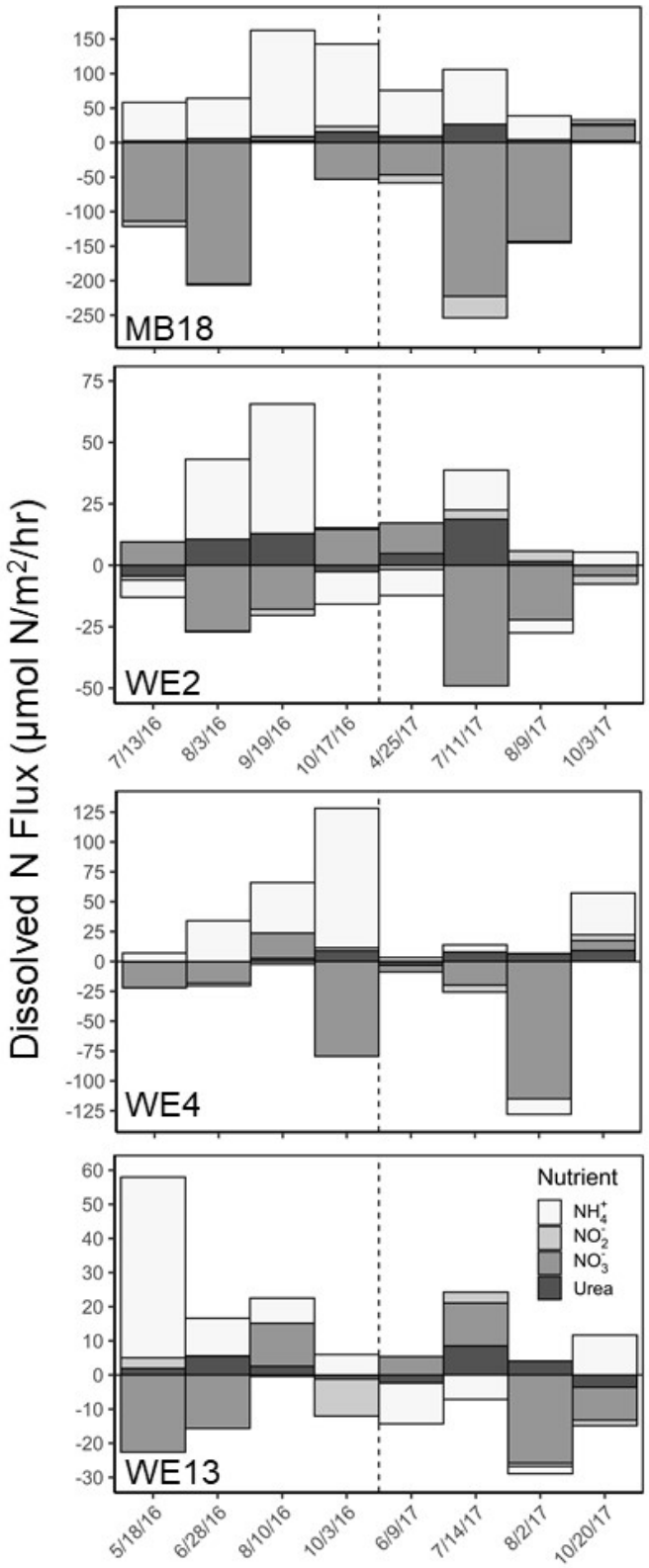
Dissolved N Flux (µmol N/m²/hr)
MB18
WE2
WE4
WE13
Nutrient
NH4+
NO2-
NO3-
Urea
7/13/16
8/3/16
9/19/16
10/17/16
4/25/17
7/11/17
8/9/17
10/3/17
5/18/16
6/28/16
8/10/16
10/3/16
6/9/17
7/14/17
8/2/17
10/20/17

Figure 3:

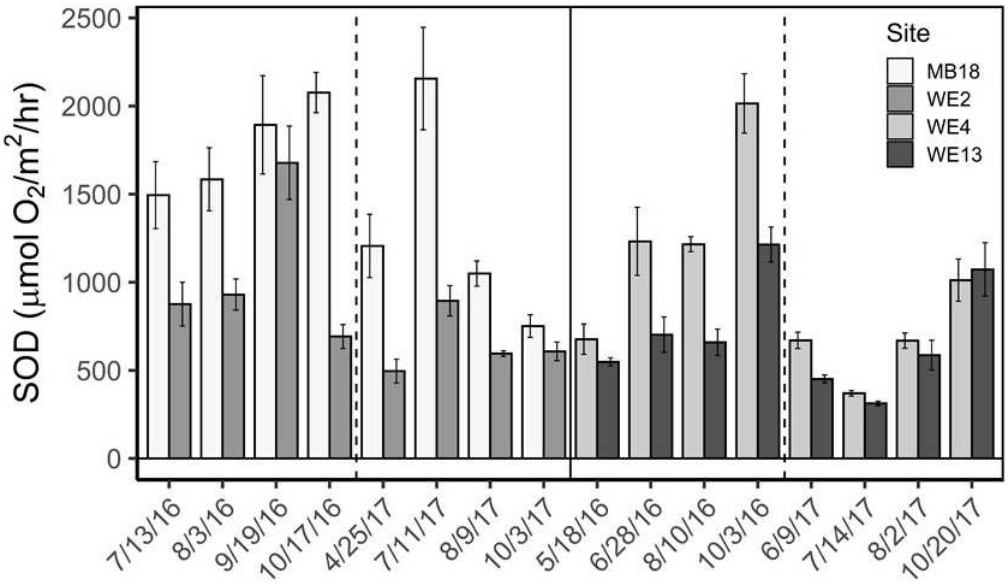
SOD (µmol O2/m2/hr)
2500
2000
1500
1000
500
0
Site
MB18
WE2
WE4
WE13
7/13/16
8/3/16
9/19/16
10/17/16
4/25/17
7/11/17
8/9/17
10/3/17
5/18/16
6/28/16
8/10/16
10/3/16
6/9/17
7/14/17
8/2/17
10/20/17

Figure 4:

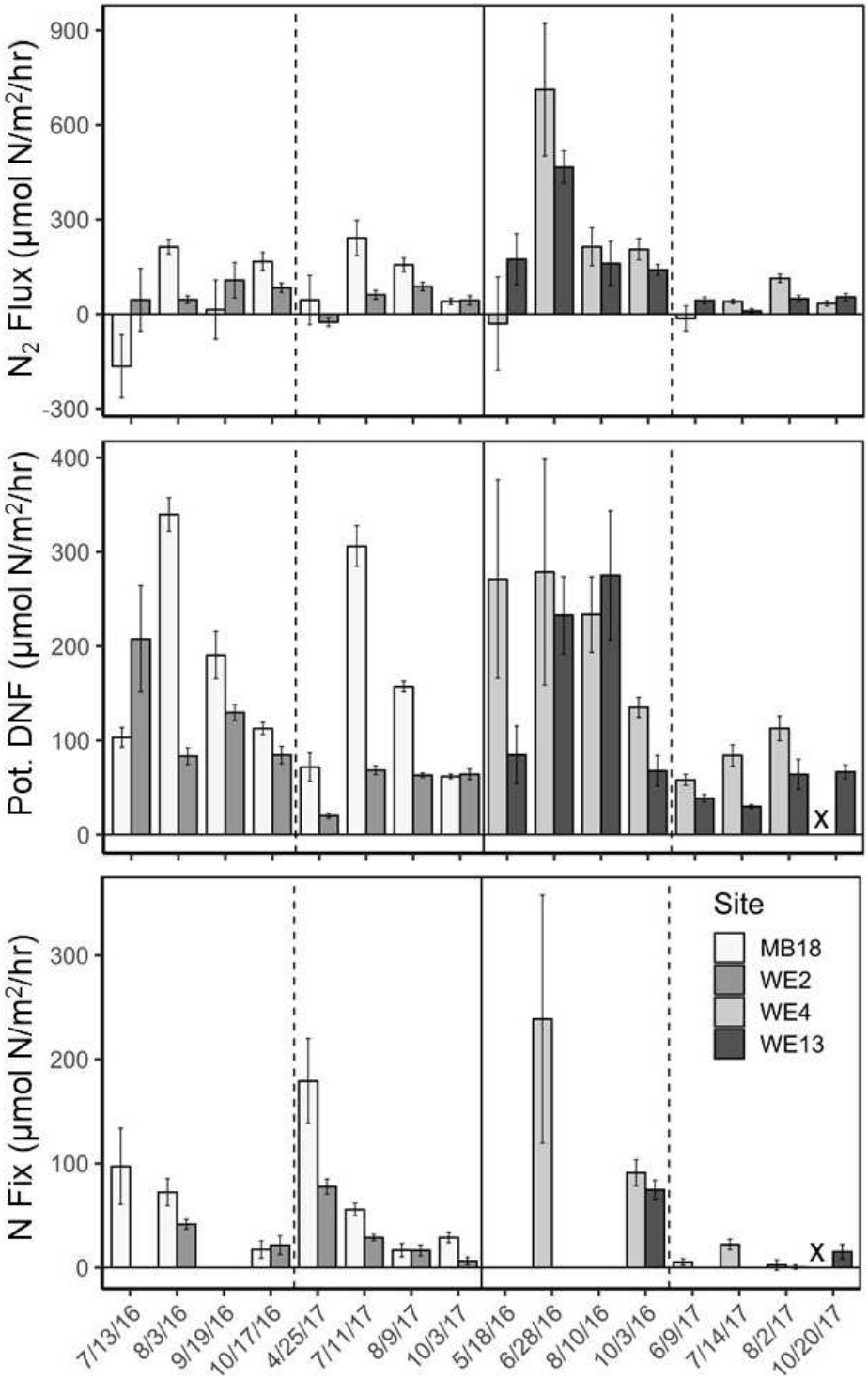
N2 Flux (µmol N/m2/hr)
900
600
300
0
-300
Pot. DNF (µmol N/m2/hr)
400
300
200
100
0
X
N Fix (µmol N/m2/hr)
300
200
100
0
X
Site
MB18
WE2
WE4
WE13
7/13/16
8/3/16
9/19/16
10/17/16
4/25/17
7/11/17
8/9/17
10/3/17
5/18/16
6/28/16
8/10/16
10/3/16
6/9/17
7/14/17
8/2/17
10/20/17

Figure 5:

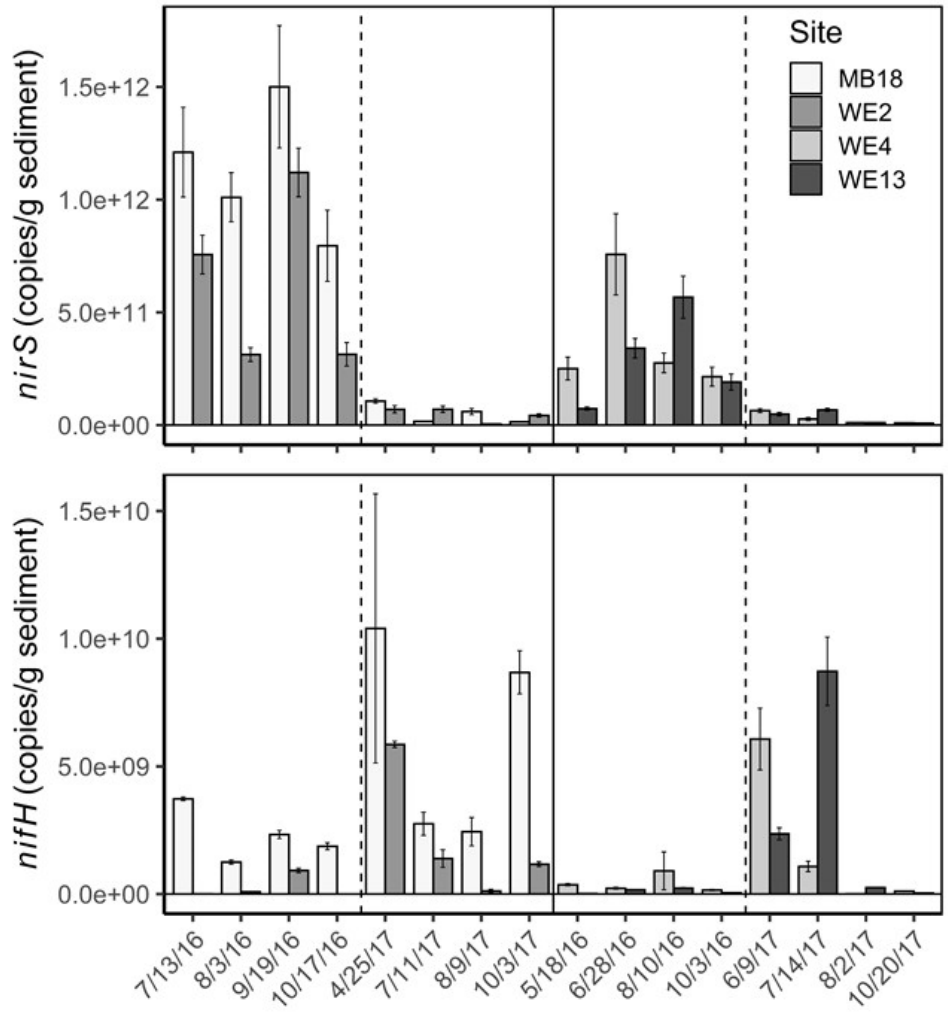
Site
MB18
WE2
WE4
WE13
nirS (copies/g sediment)
1.5e+12
1.0e+12
5.0e+11
0.0e+00
nifH (copies/g sediment)
1.5e+10
1.0e+10
5.0e+09
0.0e+00
7/13/16
8/3/16
9/19/16
10/17/16
4/25/17
7/11/17
8/9/17
10/3/17
5/18/16
6/28/16
8/10/16
10/3/16
6/9/17
7/14/17
8/2/17
10/20/17

Figure 6:

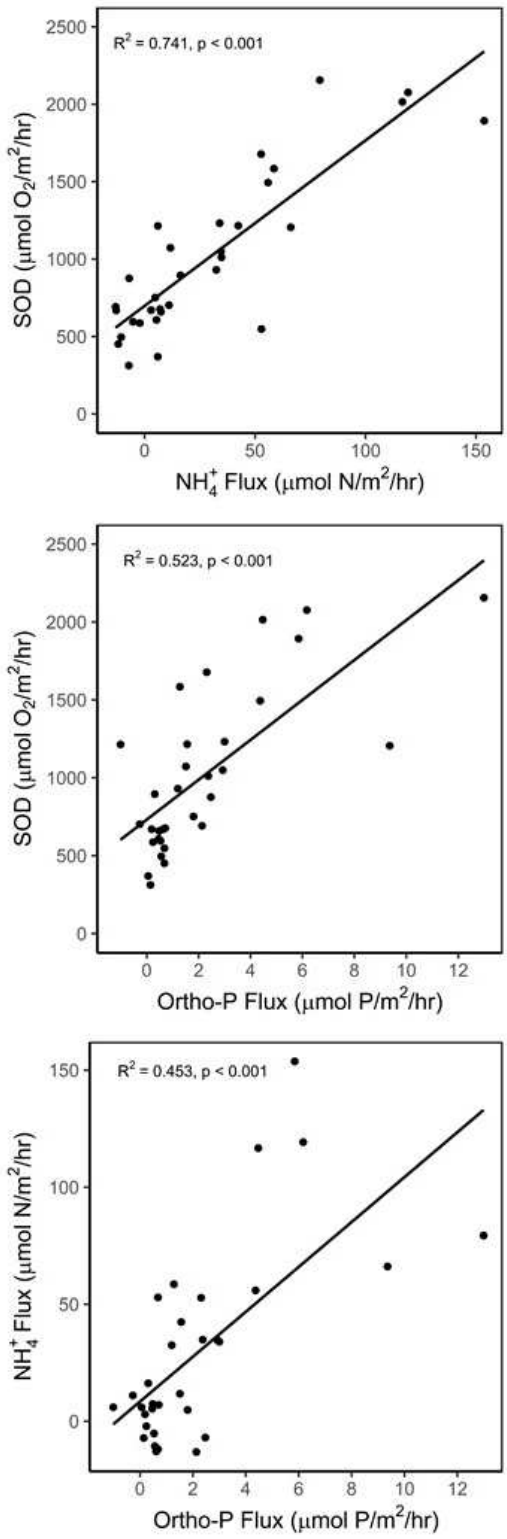
R² = 0.741, p < 0.001
SOD (µmol O2/m²/hr)
NH4+ Flux (µmol N/m²/hr)
R² = 0.523, p < 0.001
SOD (µmol O2/m²/hr)
Ortho-P Flux (µmol P/m²/hr)
R² = 0.453, p < 0.001
NH4+ Flux (µmol N/m²/hr)
Ortho-P Flux (µmol P/m²/hr)

Figure 7:

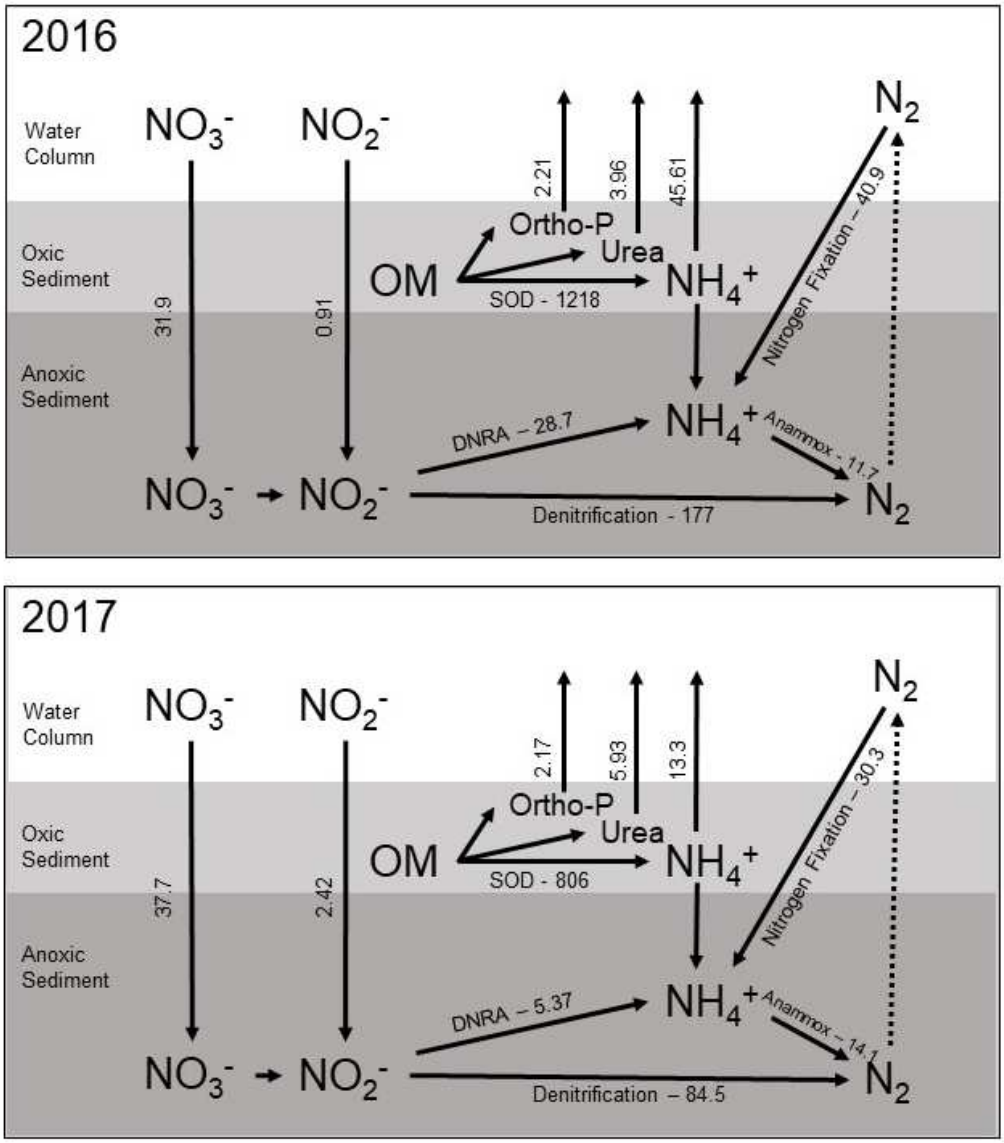
2016
Water Column
Oxic Sediment
Anoxic Sediment
NO3-
NO2-
OM
Ortho-P
Urea
SOD - 1218
NH4+
N2
2.21
3.96
45.61
31.9
0.91
Nitrogen Fixation – 40.9
DNRA – 28.7
Anammox - 11.7
Denitrification - 177
2017
Water Column
Oxic Sediment
Anoxic Sediment
NO3-
NO2-
OM
Ortho-P
Urea
SOD - 806
NH4+
N2
2.17
5.93
13.3
37.7
2.42
Nitrogen Fixation – 30.3
DNRA – 5.37
Anammox – 14.1
Denitrification – 84.5